

Fermi-surface-engineered unconventional superfluid states in a driven-dissipative non-equilibrium Fermi gas

Taira Kawamura,¹ Ryo Hanai,² and Yoji Ohashi¹

¹*Department of Physics, Keio University, 3-14-1 Hiyoshi, Kohoku-ku, Yokohama 223-8522, Japan*

²*Asia Pacific Center for Theoretical Physics, Pohang 37673, Korea*

(Dated: November 5, 2021)

We develop a theory to describe the dynamics of a driven-dissipative many-body Fermi system, to pursue our proposal to realize exotic quantum states based on reservoir engineering. Our idea is to design the shape of a Fermi surface so as to have multiple Fermi edges, by properly attaching multiple reservoirs with different chemical potentials to a fermionic system. These emerged edges give rise to additional scattering channels that can destabilize the system into unconventional states, which is exemplified in this work by considering a driven-dissipative attractively interacting Fermi gas. By formulating a quantum kinetic equation using the Nambu-Keldysh Green's function technique, we determine the nonequilibrium steady state of this system and assess its stability. We find that, besides the BCS-type isotropic pairing state, an anisotropic superfluid state being accompanied by Cooper pairs with non-zero center-of-mass momentum exists as a stable solution, even in the absence of a magnetic Zeeman field. Our result implies a great potential of realizing quantum matter beyond the equilibrium paradigm, by engineering the shape and topology of Fermi surfaces in both electronic and atomic systems.

I. INTRODUCTION

The last two decades had witnessed great progress in understanding and controlling many-body systems out of equilibrium [1–9]. When the system is driven out of equilibrium, restrictions such as the dissipation fluctuation theorem are generally lifted. The lack of these constraints gives additional “free hands” for the system to exhibit exotic states that are otherwise prohibited in equilibrium. Floquet time crystals [10–15], light-induced superconducting-like states [16–18], long-range orders in two dimension [19, 20] as well as non-reciprocal phase transitions [21–25], are a few of such examples. Among these, the strategy of dissipatively controlling many-body states by carefully designing the coupling between reservoirs and a system, which is often referred to as ‘reservoir engineering’, is recognized as a promising route to obtain the desired state [26–32]. For example, by an appropriate design of reservoir-system coupling, it is shown to be possible to implement a non-trivial topological state [26], universal quantum computing [27] as well as non-reciprocal coupling [30]. Although most of the work considers Markovian reservoirs, a non-Markovian reservoir is found to also be useful as a dissipative stabilizer of strongly correlated states, such as the Mott insulator [31] and fractional quantum Hall state [32].

In this paper, we apply non-Markovian reservoir engineering to a many-body Fermi system. In particular, we propose to design the shape of a Fermi surface by attaching multiple reservoirs with different chemical potentials μ_α to the main system, to induce an unconventional many-body state as a nonequilibrium steady state. As schematically shown in Fig. 1, the two reservoirs imprint a two-edges on the Fermi momentum distribution in the main system, arising from each reservoir chemical potential. (See the pop-up in Fig. 1.) As a result, the emerged

structure effectively works like multiple Fermi surfaces, providing additional scattering channels that can trigger the destabilization of the system into an unconventional state.

Although we expect our scheme to work for generic Fermi systems, as a paradigmatic example, we consider here an attractively interacting Fermi gas as our main system. In the accompanying paper [33], we predicted that an unconventional Fermi condensate may be realized in this non-equilibrium system, when $T_{\text{env}} = 0$ [34]. In this paper, in addition to providing the full description of our analysis, we extend Ref. [33] to the case with $T_{\text{env}} > 0$, to explore possible non-equilibrium superfluid states within the mean-field level. We also present detailed stability analyses of these mean-field superfluid solutions. This is done by examining the time evolution of the order parameter under the initial condition that it slightly deviates from the mean-field value. If the deviation always decays over time, this non-equilibrium superfluid state is judged to be stable. On the other hand, the growth of the deviation with increasing time means the instability of this state against fluctuations around the mean-field solution. In addition, when two states satisfy the stability criterion, we judge that a bistability phenomenon occurs.

Our principal results are captured in Fig. 2. Panel (a) shows the steady-state phase diagram of a driven-dissipative Fermi gas, with respect to half the chemical potential difference $\delta\mu = [\mu_L - \mu_R]/2$ between the two reservoirs, the atomic damping rate γ coming from the system-reservoir couplings, and the environment temperature T_{env} . In this phase diagram, NBCS is similar to the conventional thermal equilibrium Bardeen-Cooper-Schrieffer (BCS) state. On the other hand, NFF has a spatially oscillating order parameter, and Cooper pairs in this superfluid state have non-zero center-of-mass momentum. These characters are the same as those in the

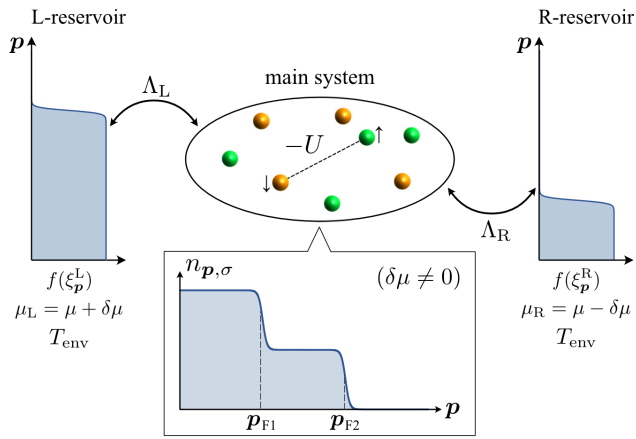


FIG. 1. Model non-equilibrium driven-dissipative two-component Fermi gas with an s -wave pairing interaction $-U (< 0)$. The main system is coupled with two reservoirs ($\alpha = L, R$) with different chemical potentials $\mu_L = \mu + \delta\mu$ and $\mu_R = \mu - \delta\mu$. Both the reservoirs consist of free fermions in the thermal equilibrium state at the environment temperature T_{env} . $f(\xi_p^\alpha)$ is the Fermi distribution function, where ξ_p^α is the kinetic energy, measured from μ_α . Λ_α describes tunneling between the main system and the α -reservoir. The pumping and decay of Fermi atoms by the two reservoirs bring about two edges at $p_{F1} = \sqrt{2m\mu_R}$ and $p_{F2} = \sqrt{2m\mu_L}$ in the Fermi momentum distribution $n_{p,\sigma}$ in the main system (where $\sigma = \uparrow, \downarrow$ describe two atomic hyperfine states).

Fulde-Ferrell (FF) state discussed in superconductivity under an external magnetic field [35–38]. However, while the Zeeman splitting between \uparrow -spin and \downarrow -spin Fermi surfaces is crucial for the FF state (where Cooper pairs are formed between \uparrow -spin electrons around the larger Fermi surface and \downarrow -spin electrons around the smaller Fermi surface), NFF appears in the spin-balanced case. This FF-like state is stabilized by the two-edge structure of the Fermi momentum distribution $n_{p,\sigma}$ (see Fig. 1), which is produced by the pumping and decay of atoms by the two reservoirs [39]. The two edges at $p_{F1} = \sqrt{2m\mu_R}$ and $p_{F2} = \sqrt{2m\mu_L}$ then work like two Fermi surfaces with different sizes, and Cooper pairs (A) and (B) in Fig. 2(b) are formed. We also see in Fig. 2(a) that, in the region where NFF is stable, NBCS is also stable (bistability).

This paper is organized as follows. In Sec. II, we extend the BCS theory to the non-equilibrium steady state, by employing the Nambu-Keldysh Green's function technique. In Sec. III, using the same technique, we derive a quantum kinetic equation to evaluate the time evolution of the superfluid order parameter, under the initial condition that it slightly deviates from the mean-field value. We show our results in Sec. IV. We first show possible mean-field solutions for non-equilibrium superfluid steady states. We then assess their stability from the time evolution of the superfluid order parameter, to draw the phase diagram in Fig. 2(a). Throughout this paper, we set $\hbar = k_B = 1$, and the system volume V is taken to be unity, for simplicity.

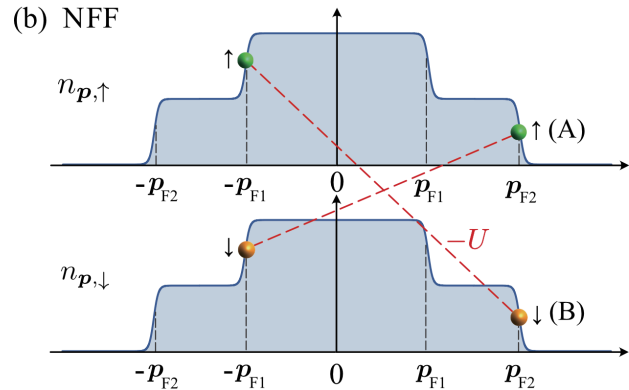
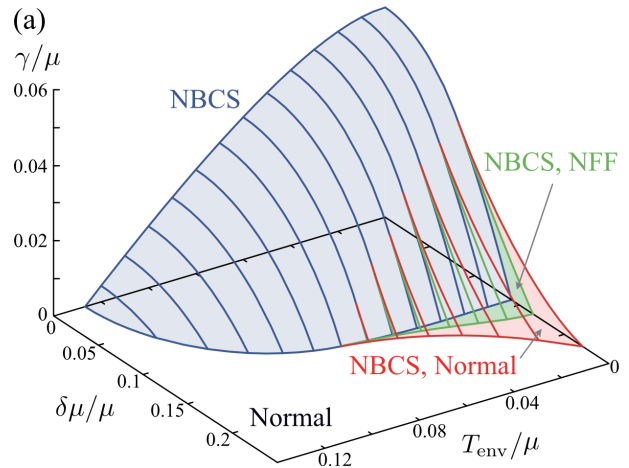


FIG. 2. (a) Steady-state phase diagram of a driven-dissipative two-component Fermi gas, with respect to half the chemical potential difference $\delta\mu = [\mu_L - \mu_R]/2$ between the two reservoirs, and the damping rate γ caused by system-reservoir couplings, and the environment temperature T_{env} (that are all scaled by the averaged chemical potential $\mu = [\mu_L + \mu_R]/2$). This figure shows the weak-coupling case when $(p_F a_s)^{-1} = -1$ (where $p_F = \sqrt{2m\mu}$) under the vanishing current condition, $\mathbf{J}_{\text{net}} = 0$. In the phase diagram, NBCS and NFF represent the non-equilibrium BCS ($\mathbf{Q} = 0$) and FF like ($\mathbf{Q} \neq 0$) states, where \mathbf{Q} is the center-of-mass momentum of a Cooper pair. (b) Schematic NFF pairing. The two-edge structure of the Fermi momentum distribution $n_{p,\sigma=\uparrow,\downarrow}$ at $p_{F1} = \sqrt{2m\mu_R}$ and $p_{F2} = \sqrt{2m\mu_L}$ works as if the system has two Fermi surfaces with different sizes, and NFF Cooper pairs are formed between (A) $|\mathbf{p}_{F2,\uparrow}\rangle$ and $|\mathbf{p}_{F1,\downarrow}\rangle$, and (B) $|\mathbf{p}_{F2,\downarrow}\rangle$ and $|\mathbf{p}_{F1,\uparrow}\rangle$.

II. BCS THEORY OF NON-EQUILIBRIUM SUPERFLUID STEADY STATE

A. Model driven-dissipative non-equilibrium Fermi gas

The model driven-dissipative two-component Fermi gas shown in Fig. 1 is described by the Hamiltonian,

$$H = H_{\text{sys}} + H_{\text{env}} + H_{\text{mix}}, \quad (1)$$

where each term has the form, in the Nambu representation [40, 41],

$$H_{\text{sys}} = - \int d\mathbf{r} \Psi^\dagger(\mathbf{r}) \frac{\nabla_{\mathbf{r}}^2}{2m} \tau_3 \Psi(\mathbf{r}) - U \int d\mathbf{r} \Psi^\dagger(\mathbf{r}) \tau_+ \Psi(\mathbf{r}) \Psi^\dagger(\mathbf{r}) \tau_- \Psi(\mathbf{r}), \quad (2)$$

$$H_{\text{env}} = \sum_{\alpha=L,R} \int d\mathbf{R} \Phi_\alpha^\dagger(\mathbf{R}) \left[-\frac{\nabla_{\mathbf{R}}^2}{2m} - \mu_\alpha \right] \tau_3 \Phi_\alpha(\mathbf{R}), \quad (3)$$

$$H_{\text{mix}} = \sum_{\alpha=L,R} \sum_{i=1}^{N_t} [\Lambda_\alpha \Phi_\alpha^\dagger(\mathbf{R}_i^\alpha) e^{i\tau_3 \mu_\alpha t} \tau_3 \Psi(\mathbf{r}_i^\alpha) + \text{h.c.}]. \quad (4)$$

In these Hamiltonians,

$$\Psi(\mathbf{r}) = \begin{pmatrix} \psi_\uparrow(\mathbf{r}) \\ \psi_\downarrow(\mathbf{r}) \end{pmatrix}, \quad (5)$$

$$\Phi_\alpha(\mathbf{R}) = \begin{pmatrix} \phi_{\alpha,\uparrow}(\mathbf{R}) \\ \phi_{\alpha,\downarrow}(\mathbf{R}) \end{pmatrix}, \quad (6)$$

represent the two-component Nambu fields describing fermions in the main system and the $\alpha = L, R$ reservoir, respectively (where $\psi_\sigma(\mathbf{r})$ ($\phi_{\alpha,\sigma}(\mathbf{R})$) is the annihilation operator of a fermion with pseudo-spin $\sigma = \uparrow, \downarrow$ and particle mass m in the main system (α -reservoir)). The corresponding Pauli matrices τ_i ($i = 1, 2, 3$), as well as $\tau_\pm = [\tau_1 \pm i\tau_2]/2$, act on the particle-hole space.

H_{sys} in Eq. (2) describes the main system in Fig. 1, consisting of a two-component Fermi gas with an s -wave pairing interaction $-U$ (< 0). Because H_{sys} involves the ultraviolet divergence, as usual in cold Fermi gas physics, we remove this singularity by measuring the interaction strength in terms of the s -wave scattering length a_s [42].

It is related to the pairing interaction $-U$ as

$$\frac{4\pi a_s}{m} = - \frac{U}{1 - U \sum_{\mathbf{p}} \frac{1}{2\varepsilon_{\mathbf{p}}}}, \quad (7)$$

where $\varepsilon_{\mathbf{p}} = \mathbf{p}^2/(2m)$ is the kinetic energy of a Fermi atom with an atomic mass m . In this paper, we only deal with the weak-coupling regime, by setting $(p_F a_s)^{-1} = -1$. Here, $p_F = \sqrt{2m\mu}$, where $\mu \equiv [\mu_R + \mu_L]/2$ (> 0) is the averaged chemical potential between the two reservoirs (where μ_α is the chemical potential of the α -reservoir in Fig. 1).

The two reservoirs ($\alpha = L, R$) are described by the Hamiltonian H_{env} in Eq. (3). We assume that both are huge compared to the main system, and are always in the thermal equilibrium state at the common environment temperature T_{env} . The particle occupation in each reservoir obeys the ordinary Fermi distribution function at T_{env} ,

$$f(\omega) = \frac{1}{e^{\omega/T_{\text{env}}} + 1}. \quad (8)$$

The coupling between the main system and the reservoirs is described by H_{mix} in Eq. (4) with the coupling strength $\Lambda_{\alpha=L,R}$. For simplicity, we set $\Lambda_L = \Lambda_R \equiv \Lambda$ in what follows. The particle tunneling is assumed to occur between randomly distributing spatial positions \mathbf{R}_i^α in the α -reservoir and \mathbf{r}_i in the main system [$i = 1, \dots, N_t \gg 1$]. Although this breaks the translational invariance of the main system, this symmetry property will later recover by taking the spatial average over the tunneling positions [43–45].

In Eq. (4), the factor $\exp(i\tau_3 \mu_\alpha t)$ describes the situation that the energy band in the α -reservoir is filled up to μ_α at $T_{\text{env}} = 0$, when the energy is measured from the bottom ($\varepsilon_{\mathbf{p}=0} = 0$) of the energy band in the main system [39, 46, 47]. By imposing the chemical-potential bias $\mu_L = \mu + \delta\mu$ and $\mu_R = \mu - \delta\mu$ ($\delta\mu > 0$) between the two reservoirs, we realize the non-equilibrium steady state in the main system. In this paper, we fix the value of the average chemical potential μ , and tune the non-equilibrium situation of the main system by adjusting the tunneling matrix element Λ , as well as the chemical-potential bias $\delta\mu$.

B. Non-equilibrium Nambu-Keldysh Green's function

To deal with the non-equilibrium superfluid state in the main system, we conveniently employ the 4×4 matrix Nambu-Keldysh Green's function [48, 49], given by

$$\hat{\mathcal{G}}(1, 2) = \begin{pmatrix} \mathcal{G}^R(1, 2) & \mathcal{G}^K(1, 2) \\ 0 & \mathcal{G}^A(1, 2) \end{pmatrix} = \begin{pmatrix} -i\Theta(t_1 - t_2) \langle [\Psi(1) \diamond \Psi^\dagger(2)]_+ \rangle & -i \langle [\Psi(1) \diamond \Psi^\dagger(2)]_- \rangle \\ 0 & i\Theta(t_2 - t_1) \langle [\Psi(1) \diamond \Psi^\dagger(2)]_+ \rangle \end{pmatrix}, \quad (9)$$

where $\Theta(t)$ is the step function, and the abbreviated notations $1 \equiv (\mathbf{r}_1, t_1)$ and $2 \equiv (\mathbf{r}_2, t_2)$ are used. In Eq. (9), \mathcal{G}^R , \mathcal{G}^A , and \mathcal{G}^K are the 2×2 matrix retarded, advanced, and Keldysh Green's functions in the two-component Nambu space, respectively. In Eq. (9),

$$[\Psi(1) \diamond \Psi^\dagger(2)]_\pm = \Psi(1) \diamond \Psi^\dagger(2) \pm \Psi^\dagger(2) \diamond \Psi(1), \quad (10)$$

where “ \diamond ” denotes the operation,

$$\Psi(1) \diamond \Psi^\dagger(2) = \begin{pmatrix} \psi_\uparrow(1)\psi_\uparrow^\dagger(2) & \psi_\uparrow(1)\psi_\downarrow(2) \\ \psi_\downarrow^\dagger(1)\psi_\uparrow^\dagger(2) & \psi_\downarrow^\dagger(1)\psi_\downarrow(2) \end{pmatrix}, \quad (11)$$

$$\Psi^\dagger(2) \diamond \Psi(1) = \begin{pmatrix} \psi_\uparrow^\dagger(2)\psi_\uparrow(1) & \psi_\downarrow(2)\psi_\uparrow(1) \\ \psi_\uparrow^\dagger(2)\psi_\downarrow(1) & \psi_\downarrow(2)\psi_\downarrow(1) \end{pmatrix}. \quad (12)$$

For later convenience, we also introduce the 4×4 matrix lesser Green's function $\mathcal{G}^<(1, 2)$, which is related to $\mathcal{G}^{R,K,A}(1, 2)$ as

$$\mathcal{G}^<(1, 2) = i \langle \Psi^\dagger(2) \diamond \Psi(1) \rangle = \frac{1}{2} [\mathcal{G}^K(1, 2) - \mathcal{G}^R(1, 2) + \mathcal{G}^A(1, 2)]. \quad (13)$$

We briefly note that the diagonal and off-diagonal components of $\mathcal{G}^<$ are related to the particle density and the pair amplitude, respectively.

In the Nambu-Keldysh scheme, effects of the pairing interaction $-U$ and the system-reservoir couplings $\Lambda_{\alpha=L,R}$ can be summarized by the 4×4 matrix self-energy correction,

$$\hat{\Sigma}(1, 2) = \begin{pmatrix} \Sigma^R(1, 2) & \Sigma^K(1, 2) \\ 0 & \Sigma^A(1, 2) \end{pmatrix} = \hat{\Sigma}_{\text{int}}(1, 2) + \hat{\Sigma}_{\text{env}}(1, 2), \quad (14)$$

which appears in the non-equilibrium Nambu-Keldysh Dyson equation [48, 49],

$$\hat{\mathcal{G}}(1, 2) = \hat{\mathcal{G}}_0(1, 2) + [\hat{\mathcal{G}}_0 \circ \hat{\Sigma} \circ \hat{\mathcal{G}}](1, 2). \quad (15)$$

Here,

$$[A \circ B](1, 2) = \int d\mathbf{r}_3 \int_{-\infty}^{\infty} dt_3 A(\mathbf{r}_1, t_1, \mathbf{r}_3, t_3) B(\mathbf{r}_3, t_3, \mathbf{r}_2, t_2) = \int d3 A(1, 3) B(3, 2), \quad (16)$$

and

$$\begin{aligned} \hat{\mathcal{G}}_0(1, 2) &= \sum_{\mathbf{p}} \int \frac{d\omega}{2\pi} e^{i\mathbf{p} \cdot (\mathbf{r}_1 - \mathbf{r}_2) - i\omega(t_1 - t_2)} \hat{\mathcal{G}}_0(\mathbf{p}, \omega) \\ &= \sum_{\mathbf{p}} \int \frac{d\omega}{2\pi} e^{i\mathbf{p} \cdot (\mathbf{r}_1 - \mathbf{r}_2) - i\omega(t_1 - t_2)} \begin{pmatrix} \frac{1}{\omega_+ - \varepsilon_{\mathbf{p}}\tau_3} & -2\pi i \delta(\omega - \varepsilon_{\mathbf{p}}) [1 - 2f_{\text{ini}}(\omega)] \\ 0 & \frac{1}{\omega_- - \varepsilon_{\mathbf{p}}\tau_3} \end{pmatrix} \end{aligned} \quad (17)$$

is the bare Green's function in the *initial* thermal equilibrium state at $t = -\infty$, where the system-reservoir couplings $\Lambda_{\alpha=L,R}$, as well as the pairing interaction $-U$, were absent. (Note that $\hat{\mathcal{G}}_0(1, 2)$ only depends on the relative coordinate as $\hat{\mathcal{G}}_0(1, 2) = \hat{\mathcal{G}}_0(1 - 2)$.) In Eq. (17), $\omega_\pm = \omega \pm i\delta$ (where δ is an infinitesimally small positive number), and $f_{\text{ini}}(\omega) = 1/[e^{\omega/T_{\text{ini}}} + 1]$ is the Fermi distribution function with T_{ini} being the initial temperature of the main system at $t = -\infty$. Although the Dyson equation (15) looks like depending on the initial state through $\hat{\mathcal{G}}_0(1, 2)$, we will soon find that the dressed Green's function $\hat{\mathcal{G}}(1, 2)$ in the final non-equilibrium steady state, which we are interested in, actually loses the initial memory [39, 43–45, 47, 50–52].

In Eq. (14), $\hat{\Sigma}_{\text{int}}$ and $\hat{\Sigma}_{\text{env}}$ describe effects of the pairing interaction $-U$ and the system-reservoir couplings $\Lambda_{\alpha=L,R}$ ($= \Lambda$), respectively. In the mean-field BCS approximation [43–45], the former is diagrammatically drawn as Fig. 3(a), which gives

$$\begin{aligned} \hat{\Sigma}_{\text{int}}(1, 2) &= iU \sum_{s=\pm} \sum_{\alpha=1,2} (\tau_s \otimes \eta_\alpha^+) \text{Tr}_N \text{Tr}_K [(\tau_{-s} \otimes \eta_\alpha^-) \hat{\mathcal{G}}(1, 2)] \delta(1 - 2) \\ &= \frac{iU}{2} \sum_{s=\pm} \begin{pmatrix} \tau_s \text{Tr}_N [\tau_{-s} \mathcal{G}^K(1, 2)] & \tau_s \text{Tr}_N [\tau_{-s} \mathcal{G}^R(1, 2) + \tau_{-s} \mathcal{G}^A(1, 2)] \\ \tau_s \text{Tr}_N [\tau_{-s} \mathcal{G}^R(1, 2) + \tau_{-s} \mathcal{G}^A(1, 2)] & \tau_s \text{Tr}_N [\tau_{-s} \mathcal{G}^K(1, 2)] \end{pmatrix} \delta(1 - 2). \end{aligned} \quad (18)$$

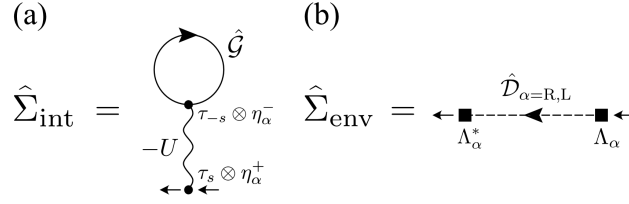


FIG. 3. Self-energy corrections. (a) $\hat{\Sigma}_{\text{int}}$ describes effects of the pairing interaction $-U$ in the mean-field BCS approximation. The solid line is the dressed Nambu-Keldysh Green's function $\hat{\mathcal{G}}$ in the main system. The wavy line is the pairing interaction $-U$, which is accompanied by the vertices $\tau_{\pm s} \otimes \eta_{\alpha}^{\pm}$ at both ends (where $s = \pm$), acting on the Nambu \otimes Keldysh space. (b) $\hat{\Sigma}_{\text{env}}$ describes effects of the system-reservoir couplings $\Lambda_{\alpha=L,R}$ in the second-order Born approximation. The dashed line is the Green's function $\hat{\mathcal{D}}_{\alpha=L,R}$ in the α -reservoir. The solid square represents the tunneling matrix $\Lambda_{\alpha=L,R}$ between the system and the α -reservoir.

Here,

$$\eta_{\alpha}^{+} = \frac{1}{\sqrt{2}}\sigma_{2-\alpha}, \quad \eta_{\alpha}^{-} = \frac{1}{\sqrt{2}}\sigma_{\alpha-1} \quad (19)$$

are vertex matrices [39], where $\sigma_{i=1,2,3}$ are the Pauli matrices acting on the Keldysh space. Tr_{N} and Tr_{K} stand for taking the trace over the Nambu and the Keldysh space, respectively.

We introduce the superfluid order parameter $\Delta(\mathbf{r}_1, t_1)$, which is related to the off-diagonal component of \mathcal{G}^{K} and $\mathcal{G}^{<}$ as

$$\Delta(\mathbf{r}_1, t_1) \equiv U \langle \psi_{\downarrow}(1)\psi_{\uparrow}(1) \rangle = -\frac{iU}{2}\mathcal{G}^{\text{K}}(1, 1)_{12} = -iU\mathcal{G}^{<}(1, 1)_{12}. \quad (20)$$

Then, Eq. (18) can be simply written as

$$\hat{\Sigma}_{\text{int}}(1, 2) = \begin{pmatrix} -\Delta(1)\tau_{+} - \Delta^{*}(1)\tau_{-} & 0 \\ 0 & -\Delta(1)\tau_{+} - \Delta^{*}(1)\tau_{-} \end{pmatrix} \delta(1-2). \quad (21)$$

We note that the off-diagonal components of $\hat{\Sigma}_{\text{int}}(1, 2)$ identically vanish, because $\mathcal{G}^{\text{R(A)}}(1, 1)_{12} = \mathcal{G}^{\text{R(A)}}(1, 1)_{21} = 0$.

For the self-energy correction $\hat{\Sigma}_{\text{env}}$ in Eq. (14), we take into account the system-reservoir couplings within the second-order Born approximation, as diagrammatically shown in Fig. 3(b). Evaluation of this diagram gives

$$\begin{aligned} \hat{\Sigma}_{\text{env}}(\mathbf{p}, \mathbf{p}', t_1, t_2) &= \int d\mathbf{r}_1 \int d\mathbf{r}_2 \hat{\Sigma}_{\text{env}}(1, 2) e^{-i(\mathbf{p}\cdot\mathbf{r}_1 + \mathbf{p}'\cdot\mathbf{r}_2)} \\ &= |\Lambda|^2 \sum_{\alpha=L,R} \sum_{i,j}^{N_t} \hat{\mathcal{D}}_{\alpha}(\mathbf{R}_i^{\alpha} - \mathbf{R}_j^{\alpha}, t_1 - t_2) e^{-i\tau_3\mu_{\alpha}(t_1-t_2)} e^{-i(\mathbf{p}\cdot\mathbf{r}_i + \mathbf{p}'\cdot\mathbf{r}_j)}, \end{aligned} \quad (22)$$

where

$$\begin{aligned} \hat{\mathcal{D}}_{\alpha}(\mathbf{R}_i^{\alpha} - \mathbf{R}_j^{\alpha}, t_1 - t_2) &= \sum_{\mathbf{q}} \int \frac{d\omega}{2\pi} e^{i\mathbf{q}\cdot(\mathbf{R}_i^{\alpha} - \mathbf{R}_j^{\alpha}) - i\omega(t_1-t_2)} \hat{\mathcal{D}}_0(\mathbf{q}, \omega) \\ &= \sum_{\mathbf{q}} \int \frac{d\omega}{2\pi} e^{i\mathbf{q}\cdot(\mathbf{R}_i^{\alpha} - \mathbf{R}_j^{\alpha}) - i\omega(t_1-t_2)} \begin{pmatrix} \frac{1}{\omega_{+} - \xi_{\mathbf{q}}^{\alpha}\tau_3} & -2\pi i\delta(\omega - \xi_{\mathbf{q}}^{\alpha}) \tanh\left(\frac{\omega}{2T_{\text{env}}}\right) \\ 0 & \frac{1}{\omega_{-} - \xi_{\mathbf{q}}^{\alpha}\tau_3} \end{pmatrix} \end{aligned} \quad (23)$$

is the non-interacting Nambu-Keldysh Green's function in the α -reservoir, with $\xi_{\mathbf{q}}^{\alpha} = \varepsilon_{\mathbf{q}} - \mu_{\alpha}$ being the kinetic energy measured from the chemical potential μ_{α} . (Note that the reservoirs are assumed to be in thermal equilibrium.) When one takes the spatial averages over the randomly distributing tunneling positions \mathbf{R}_i^{α} and \mathbf{r}_i^{α} in Eq. (22), the resulting self-energy $\langle \hat{\Sigma}_{\text{env}}(\mathbf{p}, \mathbf{p}', t_1, t_2) \rangle_{\text{av}}$ recovers its translational invariance as $\langle \hat{\Sigma}_{\text{env}}(\mathbf{p}, \mathbf{p}', t_1, t_2) \rangle_{\text{av}} = \hat{\Sigma}_{\text{env}}(\mathbf{p}, t_1, t_2) \delta_{\mathbf{p}, \mathbf{p}'}$ [39, 43–45], where

$$\hat{\Sigma}_{\text{env}}(\mathbf{p}, t_1, t_2) = N_t |\Lambda|^2 \sum_{\mathbf{q}, \alpha=L,R} \hat{\mathcal{D}}_{\alpha}(\mathbf{q}, t_1 - t_2) e^{-i\mu_{\alpha}(t_1-t_2)\tau_3}. \quad (24)$$

Carrying out the Fourier transformation with respect to the relative time $t_1 - t_2$, we have

$$\hat{\Sigma}_{\text{env}}(\mathbf{p}, \omega) = N_t |\Lambda|^2 \sum_{\mathbf{q}, \alpha=L,R} \hat{\mathcal{D}}_{\alpha}(\mathbf{q}, \omega - \mu_{\alpha} \tau_3). \quad (25)$$

For simplicity, we employ the so-called wide-band-limit approximation [53], that is, we assume white reservoirs with the constant density of states $\rho_{\alpha}(\omega) \equiv \rho$. Then, replacing \mathbf{q} summation in Eq. (25) by the ξ^{α} integration, one has

$$\hat{\Sigma}_{\text{env}}(\mathbf{p}, \omega) = \begin{pmatrix} -2i\gamma\tau_0 & -2i\gamma \left[\tanh\left(\frac{\omega - \tau_3 \mu_L}{2T_{\text{env}}}\right) + \tanh\left(\frac{\omega - \tau_3 \mu_R}{2T_{\text{env}}}\right) \right] \tau_0 \\ 0 & 2i\gamma\tau_0 \end{pmatrix}. \quad (26)$$

Here,

$$\gamma = \pi N_t \rho |\Lambda|^2 \quad (27)$$

is the quasi-particle damping rate, and τ_0 is the 2×2 unit matrix acting on the particle-hole Nambu space.

C. Extension of BCS Theory to non-equilibrium steady state

In this paper, we explore stable non-equilibrium superfluid steady states, having the following type of the order parameter:

$$\Delta(\mathbf{r}, t) = \Delta_0 e^{i\mathbf{Q} \cdot \mathbf{r}} e^{-2i\mu t}. \quad (28)$$

Without loss of generality, we take $\Delta_0 > 0$. When $\mathbf{Q} = 0$, Eq. (28) describes the BCS-type uniform superfluid, which has been discussed in exciton(-polariton) systems [23, 43–45, 50–52]. When $\mathbf{Q} \neq 0$, Eq. (28) has the same form as the order parameter in the Fulde-Ferrell (FF) superfluid state, discussed in superconductivity under an external magnetic field [35, 37, 54], as well as in a spin-polarized Fermi gas [55, 56]. Although the Larkin-Ovchinnikov type solution [36], $\Delta(\mathbf{r}, t) = \Delta_0 \cos(\mathbf{Q} \cdot \mathbf{r}) e^{-2i\mu t}$, is also conceivable in our model, leaving this possibility as our future study, we only deal with the FF-type solution in this paper. Regarding this, we emphasize that the main system has *no* spin imbalance.

To treat the superfluid order parameter $\Delta(\mathbf{r}, t)$ in Eq. (28), it is convenient to formally remove time and spatial dependence from it, which is achieved by employing the following gauge transformation [48]:

$$\hat{\mathcal{G}}(1, 2) = \begin{pmatrix} \tilde{\mathcal{G}}^R(1, 2) & \tilde{\mathcal{G}}^K(1, 2) \\ 0 & \tilde{\mathcal{G}}^A(1, 2) \end{pmatrix} \equiv e^{-i\chi(1)\tau_3 \otimes \sigma_0} \hat{\mathcal{G}}(1, 2) e^{i\chi(2)\tau_3 \otimes \sigma_0}, \quad (29)$$

$$\hat{\Sigma}(1, 2) = \begin{pmatrix} \tilde{\Sigma}^R(1, 2) & \tilde{\Sigma}^K(1, 2) \\ 0 & \tilde{\Sigma}^A(1, 2) \end{pmatrix} \equiv e^{-i\chi(1)\tau_3 \otimes \sigma_0} \hat{\Sigma}(1, 2) e^{i\chi(2)\tau_3 \otimes \sigma_0}, \quad (30)$$

where

$$\chi(\mathbf{r}, t) = \frac{1}{2} \mathbf{Q} \cdot \mathbf{r} - \mu t, \quad (31)$$

and σ_0 is the 2×2 unit matrix acting on the Keldysh space. The Nambu-Keldysh Dyson equation (15) after this manipulation is given by

$$\hat{\mathcal{G}}(1, 2) = \hat{\mathcal{G}}_0(1, 2) + [\hat{\mathcal{G}}_0 \circ \hat{\Sigma} \circ \hat{\mathcal{G}}](1, 2). \quad (32)$$

Here,

$$\hat{\mathcal{G}}_0(1, 2) = \hat{\mathcal{G}}_0(1 - 2) = e^{i[\mu(t_1 - t_2) - \frac{\mathbf{Q}}{2} \cdot (\mathbf{r}_1 - \mathbf{r}_2)] \tau_3} \hat{\mathcal{G}}_0(1 - 2). \quad (33)$$

is the gauge-transformed bare Green's function. In the energy and momentum space, Eq. (32) has the form,

$$\hat{\mathcal{G}}(\mathbf{p}, \omega) = \begin{pmatrix} \tilde{\mathcal{G}}^R(\mathbf{p}, \omega) & \tilde{\mathcal{G}}^K(\mathbf{p}, \omega) \\ 0 & \tilde{\mathcal{G}}^A(\mathbf{p}, \omega) \end{pmatrix} = \hat{\mathcal{G}}_0(\mathbf{p}, \omega) + \hat{\mathcal{G}}_0(\mathbf{p}, \omega) \hat{\Sigma}(\mathbf{p}, \omega) \hat{\mathcal{G}}(\mathbf{p}, \omega), \quad (34)$$

where

$$\begin{aligned}\hat{\hat{G}}_0(\mathbf{p}, \omega) &= \int d\mathbf{r} \int dt e^{i[\omega t - \mathbf{p} \cdot \mathbf{r}]} \hat{\hat{G}}_0(\mathbf{r}, t) = \hat{\hat{G}}_0(\mathbf{p} + \frac{\mathbf{Q}}{2} \tau_3, \omega + \mu \tau_3) \\ &= \begin{pmatrix} \frac{1}{\omega + -\xi_{\mathbf{p} + (\mathbf{Q}/2)\tau_3} \tau_3} & -2\pi i \delta(\omega - \xi_{\mathbf{p} + (\mathbf{Q}/2)\tau_3} \tau_3) [1 - 2f_{\text{ini}}(\omega + \mu \tau_3)] \\ 0 & \frac{1}{\omega - \xi_{\mathbf{p} + (\mathbf{Q}/2)\tau_3} \tau_3} \end{pmatrix},\end{aligned}\quad (35)$$

with $\xi_{\mathbf{p}} = \varepsilon_{\mathbf{p}} - \mu$. The interaction component $\hat{\hat{\Sigma}}_{\text{int}}$ of the self-energy $\hat{\hat{\Sigma}} = \hat{\hat{\Sigma}}_{\text{int}} + \hat{\hat{\Sigma}}_{\text{env}}$ in Eq. (32) is obtained from Eq. (26) as

$$\hat{\hat{\Sigma}}_{\text{int}}(1, 2) = \hat{\hat{\Sigma}}_{\text{int}}(1 - 2) = \begin{pmatrix} -\Delta_0 \tau_1 & 0 \\ 0 & -\Delta_0 \tau_1 \end{pmatrix} \delta(1 - 2). \quad (36)$$

In the energy and momentum space, this self-energy has the form,

$$\hat{\hat{\Sigma}}_{\text{int}}(\mathbf{p}, \omega) = \begin{pmatrix} -\Delta_0 \tau_1 & 0 \\ 0 & -\Delta_0 \tau_1 \end{pmatrix}. \quad (37)$$

In the same manner, the self-energy $\hat{\hat{\Sigma}}_{\text{env}}(1, 2)$ coming from the system-reservoir couplings can also be obtained from Eq. (26). Thus, it has the form, in the energy and momentum space,

$$\begin{aligned}\hat{\hat{\Sigma}}_{\text{env}}(\mathbf{p}, \omega) &= \hat{\hat{\Sigma}}_{\text{env}}(\mathbf{p} + \frac{\mathbf{Q}}{2} \tau_3, \omega + \mu \tau_3) \\ &= \begin{pmatrix} -2i\gamma \tau_0 & -2i\gamma \left[\tanh\left(\frac{\omega - \delta\mu}{2T_{\text{env}}}\right) + \tanh\left(\frac{\omega + \delta\mu}{2T_{\text{env}}}\right) \right] \tau_0 \\ 0 & 2i\gamma \tau_0 \end{pmatrix}.\end{aligned}\quad (38)$$

The self-energy $\hat{\hat{\Sigma}}(\mathbf{p}, \omega)$ involved in the Dyson equation (34) is then given by the sum of Eqs. (37) and (38).

Solving the Dyson equation (34), we obtain

$$\tilde{\mathcal{G}}^{\text{R}}(\mathbf{p}, \omega) = \sum_{\eta=\pm} \frac{1}{\omega + 2i\gamma - E_{\mathbf{p}, \mathbf{Q}}^{0, \eta}} \Xi_{\mathbf{p}, \mathbf{Q}}^{0, \eta}, \quad (39)$$

$$\tilde{\mathcal{G}}^{\text{A}}(\mathbf{p}, \omega) = \sum_{\eta=\pm} \frac{1}{\omega - 2i\gamma - E_{\mathbf{p}, \mathbf{Q}}^{0, \eta}} \Xi_{\mathbf{p}, \mathbf{Q}}^{0, \eta}, \quad (40)$$

$$\tilde{\mathcal{G}}^{\text{K}}(\mathbf{p}, \omega) = \sum_{\eta=\pm} \frac{4i\gamma [1 - 2F(\omega)]}{[\omega - \eta E_{\mathbf{p}, \mathbf{Q}}^{0, \eta}]^2 + 4\gamma^2} \Xi_{\mathbf{p}, \mathbf{Q}}^{0, \eta}, \quad (41)$$

where

$$E_{\mathbf{p}, \mathbf{Q}}^{0, \pm} = \sqrt{(\xi_{\mathbf{p}, \mathbf{Q}}^{(\text{s})})^2 + \Delta_0^2} \pm \xi_{\mathbf{p}, \mathbf{Q}}^{(\text{a})} \equiv E_{\mathbf{p}, \mathbf{Q}}^0 \pm \xi_{\mathbf{p}, \mathbf{Q}}^{(\text{a})}, \quad (42)$$

$$\Xi_{\mathbf{p}, \mathbf{Q}}^{0, \pm} = \frac{1}{2} \left[\tau_0 \pm \frac{\xi_{\mathbf{p}, \mathbf{Q}}^{(\text{s})}}{E_{\mathbf{p}, \mathbf{Q}}^0} \tau_3 \mp \frac{\Delta_0}{E_{\mathbf{p}, \mathbf{Q}}^0} \tau_1 \right], \quad (43)$$

with $\xi_{\mathbf{p}, \mathbf{Q}}^{(\text{s})} = [\xi_{\mathbf{p} + \mathbf{Q}/2} + \xi_{-\mathbf{p} + \mathbf{Q}/2}]/2$, and $\xi_{\mathbf{p}, \mathbf{Q}}^{(\text{a})} = [\xi_{\mathbf{p} + \mathbf{Q}/2} - \xi_{-\mathbf{p} + \mathbf{Q}/2}]/2$. In Eq. (41),

$$F(\omega) = \frac{1}{2} [f(\omega + \delta\mu) + f(\omega - \delta\mu)] \quad (44)$$

works as the non-equilibrium distribution function in the main system (although T_{env} is used in $f(\omega)$, see Eq. (8)). When we set $\omega = \xi_{\mathbf{p}}$, the resulting momentum distribution $F(\xi_{\mathbf{p}})$ has two Fermi-surface-like edges at $p_{\text{F1}} = \sqrt{2m\mu_{\text{R}}}$ and $p_{\text{F2}} = \sqrt{2m\mu_{\text{L}}}$, as schematically drawn in Fig. 1.

The superfluid order parameter $\Delta(\mathbf{r}, t)$ in Eq. (28) is self-consistently determined from Eq. (20). To evaluate this equation, we note that the gauge-transformed lesser Green's function $\tilde{\mathcal{G}}^<(\mathbf{p}, \omega)$ in the energy and momentum space is obtained from Eqs. (13) and (39)-(41) as

$$\begin{aligned}\tilde{\mathcal{G}}^<(\mathbf{p}, \omega) &= \frac{1}{2} [\tilde{\mathcal{G}}^{\text{K}}(\mathbf{p}, \omega) - \tilde{\mathcal{G}}^{\text{R}}(\mathbf{p}, \omega) + \tilde{\mathcal{G}}^{\text{A}}(\mathbf{p}, \omega)] \\ &= \sum_{\eta=\pm} \frac{4i\gamma F(\omega)}{[\omega - \eta E_{\mathbf{p}, \mathbf{Q}}^{0, \eta}]^2 + 4\gamma^2} \Xi_{\mathbf{p}, \mathbf{Q}}^{0, \eta}.\end{aligned}\quad (45)$$

Using Eq. (45) in evaluating Eq. (20), we obtain the gap equation,

$$1 = U \sum_{\mathbf{p}} \int_{-\infty}^{\infty} \frac{d\omega}{2\pi} \frac{4\gamma[\omega - \xi_{\mathbf{p},\mathbf{Q}}^{(a)}][1 - 2F(\omega)]}{[(\omega - E_{\mathbf{p},\mathbf{Q}}^{0+})^2 + 4\gamma^2][(\omega + E_{\mathbf{p},\mathbf{Q}}^{0-})^2 + 4\gamma^2]}. \quad (46)$$

To quickly see the relation to the ordinary BCS gap equation, we take the thermal equilibrium and uniform limit, by setting $(\gamma, \delta\mu, \mathbf{Q}) \rightarrow (+0, 0, 0)$. Then, Eq. (46) is reduced to

$$1 = U \sum_{\mathbf{p}} \frac{1}{2E_{\mathbf{p}}} \tanh\left(\frac{E_{\mathbf{p}}}{2T_{\text{env}}}\right), \quad (47)$$

where $E_{\mathbf{p}} = E_{\mathbf{p},\mathbf{Q}=0}^0 = \sqrt{\xi_{\mathbf{p}}^2 + \Delta_0^2}$. Equation (47) is just the same form as the ordinary BCS gap equation [41], when one interprets μ and T_{env} as the Fermi chemical potential and the temperature in the main system, respectively. Thus, Eq. (46) may be viewed as a non-equilibrium extension of the BCS gap equation.

Because $\Delta(\mathbf{r}, t)$ in Eq. (28) involves two parameters Δ_0 and \mathbf{Q} , we actually need one more equation to completely fix these parameters [57]. For this purpose, we impose the vanishing condition for the net current \mathbf{J}_{net} in the main system. In the Nambu-Keldysh formalism, it is given by

$$\mathbf{J}_{\text{net}} = \sum_{\sigma=\uparrow,\downarrow} \sum_{\mathbf{p}} [\mathbf{p} + \mathbf{Q}/2] n_{\mathbf{p},\sigma} = 0, \quad (48)$$

where the Fermi momentum distribution $n_{\mathbf{p},\sigma}$ in the pseudo-spin σ component is related to the diagonal component of the lesser Green's function $\tilde{\mathcal{G}}^<(\mathbf{p}, \omega)$ in Eq. (45) as

$$n_{\mathbf{p},\uparrow} = -i \int_{-\infty}^{\infty} \frac{d\omega}{2\pi} \tilde{\mathcal{G}}^<(\mathbf{p}, \omega)_{11}, \quad (49)$$

$$n_{\mathbf{p},\downarrow} = 1 - i \int_{-\infty}^{\infty} \frac{d\omega}{2\pi} \tilde{\mathcal{G}}^<(-\mathbf{p}, \omega)_{22}. \quad (50)$$

We solve the gap equation (46) under the condition in Eq. (48), to self-consistently determine (Δ_0, \mathbf{Q}) for a given set $(\gamma, \delta\mu, T_{\text{env}})$ of environment parameters.

We note that the vanishing-current condition in Eq. (48) must always be satisfied in any thermodynamically stable state in the absence of an external magnetic field, which is sometimes referred to the Bloch's theorem in the literature [58, 59]. In the non-equilibrium case, on the other hand, the magnitude of the net current depends on the choice of a boundary condition. Thus, although this paper only treats the case with Eq. (48), one may also consider more general cases with $\mathbf{J}_{\text{net}} \neq 0$, as in the current-carrying BCS and FF states [60].

III. QUANTUM KINETIC THEORY TO ASSESS THE STABILITY OF NON-EQUILIBRIUM FERMION SUPERFLUIDS

A. Quantum kinetic equation

So far, we have obtained the self-consistent equations that the steady state solutions satisfy. In order to make sure that the obtained solutions are physical, we study the stability of such solutions. In this section, we explain how one can check such stability in a nonequilibrium setup.

The stability of the obtained solution can be examined by tracing the time evolution of the superfluid order parameter under the initial condition that it is slightly deviated from the mean-field value at $t = 0$. This is done here by deriving a quantum kinetic equation (QKE). We can then determine the stability of the steady-state solution by observing whether such deviation decays or grows over time.

The central quantity of interest is the Wigner-transformed Nambu lesser Green's function [48, 49], given by

$$\tilde{\mathcal{G}}^<(\mathbf{p}, \omega, \mathbf{r}, t) = \int d\mathbf{r}_r \int dt_r e^{i(\omega t_r - \mathbf{p} \cdot \mathbf{r}_r)} \tilde{\mathcal{G}}^<(\mathbf{r}_1, t_1, \mathbf{r}_2, t_2). \quad (51)$$

Here, $\mathbf{r}_r = \mathbf{r}_1 - \mathbf{r}_2$ and $\mathbf{r} = (\mathbf{r}_1 + \mathbf{r}_2)/2$ are, respectively, the relative coordinate and the center-of-mass coordinate. For time variables, we have also introduced $t_r = t_1 - t_2$ and $t = (t_1 + t_2)/2$ in Eq. (51). It is useful to study such

quantity since the off-diagonal component of this quantity is directly related to the (gauge-transformed) superfluid order parameter $\tilde{\Delta}(\mathbf{r}, t)$. This can be readily seen by summing up $\tilde{\mathcal{G}}^<(\mathbf{p}, \omega, \mathbf{r}, t)$ over momentum \mathbf{p} and frequency ω :

$$-i \sum_{\mathbf{p}} \tilde{\mathcal{G}}_{\mathbf{p}}^<(\mathbf{r}, t) \equiv -i \sum_{\mathbf{p}} \int_{-\infty}^{\infty} \frac{d\omega}{2\pi} \tilde{\mathcal{G}}^<(\mathbf{p}, \omega, \mathbf{r}, t) = \begin{pmatrix} n_{\uparrow}(\mathbf{r}, t) & \frac{\tilde{\Delta}(\mathbf{r}, t)}{U} \\ \frac{\tilde{\Delta}^*(\mathbf{r}, t)}{U} & 1 - n_{\downarrow}(\mathbf{r}, t) \end{pmatrix}, \quad (52)$$

Note that the diagonal component is directly related to the particle density $n_{\sigma}(\mathbf{r}, t)$ of the σ -spin component. Therefore, the order parameter dynamics and the stability of the steady state solutions in the superfluid phase can be examined by analyzing the dynamics of Eq. (51).

Below, we consider the dynamics of ω -integrated (and Wigner-transformed) lesser Green's function, $\tilde{\mathcal{G}}_{\mathbf{p}}^<(\mathbf{r}, t)$. Using the Dyson's equation, we arrive at [48, 61] (See Appendix A for deviation.)

$$i\partial_t \tilde{\mathcal{G}}_{\mathbf{p}}^<(\mathbf{r}, t) - [\xi_{\mathbf{p}} \tau_3, \tilde{\mathcal{G}}_{\mathbf{p}}^<(\mathbf{r}, t)]_- - \left[\frac{\mathbf{Q}^2}{8m} \tau_3, \tilde{\mathcal{G}}_{\mathbf{p}}^<(\mathbf{r}, t) \right]_- + \left[\frac{1}{8m} \tau_3, \nabla_{\mathbf{r}}^2 \tilde{\mathcal{G}}_{\mathbf{p}}^<(\mathbf{r}, t) \right]_- \\ + \frac{i}{2} \left[\frac{\mathbf{p}}{m} \tau_3, \nabla_{\mathbf{r}} \tilde{\mathcal{G}}_{\mathbf{p}}^<(\mathbf{r}, t) \right]_+ + \frac{i}{2} \left[\frac{\mathbf{Q}}{2m} \tau_0, \nabla_{\mathbf{r}} \tilde{\mathcal{G}}_{\mathbf{p}}^<(\mathbf{r}, t) \right]_+ = \mathcal{I}_{\mathbf{p}}(\mathbf{r}, t). \quad (53)$$

In Eq. (53), the collision term $\mathcal{I}_{\mathbf{p}}(\mathbf{r}, t) = \mathcal{I}_{\mathbf{p}}^{\text{int}}(\mathbf{r}, t) + \mathcal{I}_{\mathbf{p}}^{\text{env}}(\mathbf{r}, t)$ consists of the interaction term,

$$\mathcal{I}_{\mathbf{p}}^{\text{int}}(\mathbf{r}, t) = \int_{-\infty}^{\infty} \frac{d\omega}{2\pi} [\tilde{\Sigma}_{\text{int}}^{\text{R}} \circ \tilde{\mathcal{G}}^< - \tilde{\mathcal{G}}^< \circ \tilde{\Sigma}_{\text{int}}^{\text{A}} + \tilde{\Sigma}_{\text{int}}^< \circ \tilde{\mathcal{G}}^{\text{A}} - \tilde{\mathcal{G}}^{\text{R}} \circ \tilde{\Sigma}_{\text{int}}^<](\mathbf{p}, \omega, \mathbf{r}, t), \quad (54)$$

as well as the environment term,

$$\mathcal{I}_{\mathbf{p}}^{\text{env}}(\mathbf{r}, t) = \int_{-\infty}^{\infty} \frac{d\omega}{2\pi} [\tilde{\Sigma}_{\text{env}}^{\text{R}} \circ \tilde{\mathcal{G}}^< - \tilde{\mathcal{G}}^< \circ \tilde{\Sigma}_{\text{env}}^{\text{A}} + \tilde{\Sigma}_{\text{env}}^< \circ \tilde{\mathcal{G}}^{\text{A}} - \tilde{\mathcal{G}}^{\text{R}} \circ \tilde{\Sigma}_{\text{env}}^<](\mathbf{p}, \omega, \mathbf{r}, t). \quad (55)$$

In Eqs. (54) and (55), $[A \circ B](\mathbf{p}, \omega, \mathbf{r}, t)$ is the Wigner transformation of the convolution $[A \circ B](1, 2)$ in Eq. (16), which is known to be represented by [48, 49]

$$[A \circ B](\mathbf{p}, \omega, \mathbf{r}, t) = A(\mathbf{p}, \omega, \mathbf{r}, t) e^{\frac{i}{2} [\overleftarrow{\partial}_{\omega} \overrightarrow{\partial}_t - \overleftarrow{\partial}_t \overrightarrow{\partial}_{\omega} + \overleftarrow{\partial}_{\mathbf{r}} \cdot \overrightarrow{\partial}_{\mathbf{p}} - \overleftarrow{\partial}_{\mathbf{p}} \cdot \overrightarrow{\partial}_{\mathbf{r}}]} B(\mathbf{p}, \omega, \mathbf{r}, t) \\ = A(\mathbf{p}, \omega, \mathbf{r}, t) B(\mathbf{p}, \omega, \mathbf{r}, t) + \frac{i}{2} A(\mathbf{p}, \omega, \mathbf{r}, t) \left[\overleftarrow{\partial}_{\omega} \overrightarrow{\partial}_t - \overleftarrow{\partial}_t \overrightarrow{\partial}_{\omega} + \overleftarrow{\partial}_{\mathbf{r}} \cdot \overrightarrow{\partial}_{\mathbf{p}} - \overleftarrow{\partial}_{\mathbf{p}} \cdot \overrightarrow{\partial}_{\mathbf{r}} \right] B(\mathbf{p}, \omega, \mathbf{r}, t) + \dots \quad (56)$$

Here, the left (right) arrow on each differential operator means that it acts on the left (right) side of this operator. Since we are interested in the slowly varying dynamics both in terms of time and space, below, we will only retain up to the first order with respect to $\left[\overleftarrow{\partial}_{\omega} \overrightarrow{\partial}_t - \overleftarrow{\partial}_t \overrightarrow{\partial}_{\omega} + \overleftarrow{\partial}_{\mathbf{r}} \cdot \overrightarrow{\partial}_{\mathbf{p}} - \overleftarrow{\partial}_{\mathbf{p}} \cdot \overrightarrow{\partial}_{\mathbf{r}} \right]$, which greatly simplifies the analysis.

Let us first evaluate further the interaction term $\mathcal{I}_{\mathbf{p}}^{\text{int}}(\mathbf{r}, t)$ of the collision term in Eq. (54). The self-energies $\tilde{\Sigma}_{\text{int}}^{\text{R}, \text{A}, <}$ in the Wigner representation that enters $\mathcal{I}_{\mathbf{p}}^{\text{int}}(\mathbf{r}, t)$ also depend on t through $\tilde{\Delta}(\mathbf{r}, t)$ as

$$\tilde{\Sigma}_{\text{int}}^{\text{R}}(\mathbf{p}, \omega, \mathbf{r}, t) = -[\tilde{\Delta}(\mathbf{r}, t) \tau_+ + \tilde{\Delta}^*(\mathbf{r}, t) \tau_-] \equiv -\tilde{\Delta}(\mathbf{r}, t), \quad (57)$$

$$\tilde{\Sigma}_{\text{int}}^{\text{A}}(\mathbf{p}, \omega, \mathbf{r}, t) = -\tilde{\Delta}^{\dagger}(\mathbf{r}, t), \quad (58)$$

$$\tilde{\Sigma}_{\text{int}}^<(\mathbf{p}, \omega, \mathbf{r}, t) = 0. \quad (59)$$

Within the first order gradient approximation of the Moyal product mentioned above, Eq. (54) is evaluated as

$$\mathcal{I}_{\mathbf{p}}^{\text{int}}(\mathbf{r}, t) \simeq -[\tilde{\Delta}(\mathbf{r}, t), \tilde{\mathcal{G}}_{\mathbf{p}}^<(\mathbf{r}, t)]_- - \frac{i}{2} [\nabla_{\mathbf{r}} \tilde{\Delta}(\mathbf{r}, t), \partial_{\mathbf{p}} \tilde{\mathcal{G}}_{\mathbf{p}}^<(\mathbf{r}, t)]_+ + \frac{i}{2} \int_{-\infty}^{\infty} \frac{d\omega}{2\pi} [\partial_t \tilde{\Delta}(\mathbf{r}, t), \partial_{\omega} \tilde{\mathcal{G}}^<(\mathbf{p}, \omega, \mathbf{r}, t)]_+ \\ = -[\tilde{\Delta}(\mathbf{r}, t), \tilde{\mathcal{G}}_{\mathbf{p}}^<(\mathbf{r}, t)]_- - \frac{i}{2} [\nabla_{\mathbf{r}} \tilde{\Delta}(\mathbf{r}, t), \nabla_{\mathbf{p}} \tilde{\mathcal{G}}_{\mathbf{p}}^<(\mathbf{r}, t)]_+, \quad (60)$$

where the last term in the first expression vanishes by the integration by parts.

For the environment part $\mathcal{I}_{\mathbf{p}}^{\text{env}}(\mathbf{r}, t)$ of the collision term in Eq. (55), we take advantage of the fact that the reservoirs are assumed to be huge compared to the main system and remain unchanged. Because of this property, the self energy

$\hat{\Sigma}_{\text{env}}^{\leq}(\mathbf{p}, \omega)$ that enters $\mathcal{I}_{\mathbf{p}}^{\text{env}}(\mathbf{r}, t)$ can be expressed as,

$$\tilde{\Sigma}_{\text{env}}^{\text{R}}(\mathbf{p}, \omega, \mathbf{r}, t) = -2i\gamma\tau_0, \quad (61)$$

$$\tilde{\Sigma}_{\text{env}}^{\text{A}}(\mathbf{p}, \omega, \mathbf{r}, t) = 2i\gamma\tau_0, \quad (62)$$

$$\tilde{\Sigma}_{\text{env}}^{\leq}(\mathbf{p}, \omega, \mathbf{r}, t) = 4i\gamma F(\omega)\tau_0, \quad (63)$$

which are actually the same as the steady-state counterpart given in Eq. (38). Substituting these into Eq. (55), we obtain, again within the first-order gradient expansion,

$$\mathcal{I}_{\mathbf{p}}^{\text{env}}(\mathbf{r}, t) \simeq -4i\gamma\tilde{\mathcal{G}}_{\mathbf{p}}^{\leq}(\mathbf{r}, t) - 4\gamma \int_{-\infty}^{\infty} \frac{d\omega}{2\pi} F(\omega) \mathcal{A}(\mathbf{p}, \omega, \mathbf{r}, t) + 4\gamma \int_{-\infty}^{\infty} \frac{d\omega}{2\pi} \partial_{\omega} F(\omega) \partial_t \mathcal{R}(\mathbf{p}, \omega, \mathbf{r}, t), \quad (64)$$

where we have introduced the spectral weight [48],

$$\mathcal{A}(\mathbf{p}, \omega, \mathbf{r}, t) = i[\tilde{\mathcal{G}}^{\text{R}} - \tilde{\mathcal{G}}^{\text{A}}](\mathbf{p}, \omega, \mathbf{r}, t), \quad (65)$$

and

$$\mathcal{R}(\mathbf{p}, \omega, \mathbf{r}, t) = \frac{1}{2}[\tilde{\mathcal{G}}^{\text{R}} + \tilde{\mathcal{G}}^{\text{A}}](\mathbf{p}, \omega, \mathbf{r}, t). \quad (66)$$

As shown in Appendix B, the last term in Eq. (64) vanishes in the present case. Thus, we obtain

$$\mathcal{I}_{\mathbf{p}}^{\text{env}}(\mathbf{r}, t) = -4i\gamma\tilde{\mathcal{G}}_{\mathbf{p}}^{\leq}(\mathbf{r}, t) - 4\gamma \int_{-\infty}^{\infty} \frac{d\omega}{2\pi} F(\omega) \mathcal{A}(\mathbf{p}, \omega, \mathbf{r}, t). \quad (67)$$

Using the expressions for $\tilde{\mathcal{G}}^{\text{R}}(\mathbf{p}, \omega, \mathbf{r}, t)$ and $\tilde{\mathcal{G}}^{\text{A}}(\mathbf{p}, \omega, \mathbf{r}, t)$ given, respectively, in Eqs. (B4) and (B5), one finds that the time-dependent spectral function $\mathcal{A}(\mathbf{p}, \omega, \mathbf{r}, t)$ in Eq. (65) has the form,

$$\mathcal{A}(\mathbf{p}, \omega, \mathbf{r}, t) = \sum_{\eta=\pm} \frac{4\gamma}{[\omega - E_{\mathbf{p}, \mathbf{Q}}^{\eta}(\mathbf{r}, t)]^2 + 4\gamma^2} \Xi_{\mathbf{p}, \mathbf{Q}}^{\eta}(\mathbf{r}, t), \quad (68)$$

where $E_{\mathbf{p}, \mathbf{Q}}^{\pm}(\mathbf{r}, t)$ and $\Xi_{\mathbf{p}, \mathbf{Q}}^{\eta}(\mathbf{r}, t)$ are given in Eqs. (B6) and (B7), respectively.

Substituting Eqs. (60) and (67) into Eq. (53), we obtain the desired QKE,

$$\begin{aligned} i\partial_t \tilde{\mathcal{G}}_{\mathbf{p}}^{\leq}(\mathbf{r}, t) &= [\xi_{\mathbf{p}}\tau_3 - \tilde{\Delta}(\mathbf{r}, t), \tilde{\mathcal{G}}_{\mathbf{p}}^{\leq}(\mathbf{r}, t)]_- + \left[\frac{\mathbf{Q}^2}{8m}\tau_3, \tilde{\mathcal{G}}_{\mathbf{p}}^{\leq}(\mathbf{r}, t) \right]_- - \left[\frac{1}{8m}\tau_3, \nabla_{\mathbf{r}}^2 \tilde{\mathcal{G}}_{\mathbf{p}}^{\leq}(\mathbf{r}, t) \right]_- \\ &\quad - \frac{i}{2} \left[\frac{\mathbf{p}}{m}\tau_3, \nabla_{\mathbf{r}} \tilde{\mathcal{G}}_{\mathbf{p}}^{\leq}(\mathbf{r}, t) \right]_+ - \frac{i}{2} \left[\frac{\mathbf{Q}}{2m}\tau_0, \nabla_{\mathbf{r}} \tilde{\mathcal{G}}_{\mathbf{p}}^{\leq}(\mathbf{r}, t) \right]_+ \\ &\quad - 4i\gamma\tilde{\mathcal{G}}_{\mathbf{p}}^{\leq}(\mathbf{r}, t) - 4\gamma \int_{-\infty}^{\infty} \frac{d\omega}{2\pi} F(\omega) \mathcal{A}(\mathbf{p}, \omega, \mathbf{r}, t) \\ &\quad - \frac{i}{2} [\nabla_{\mathbf{r}} \tilde{\Delta}(\mathbf{r}, t), \nabla_{\mathbf{p}} \tilde{\mathcal{G}}_{\mathbf{p}}^{\leq}(\mathbf{r}, t)]_+. \end{aligned} \quad (69)$$

In fact, the last term does not actually affect the time evolution of the superfluid order parameter $\bar{\Delta}(\mathbf{r}, t)$. To see this, we recall that $\bar{\Delta}(\mathbf{r}, t)$ is related to the (gauge-transformed) lesser Green's function as

$$\bar{\Delta}(\mathbf{r}, t) = -iU \sum_{\mathbf{p}} \tilde{\mathcal{G}}_{\mathbf{p}}^{\leq}(\mathbf{r}, t)_{12}. \quad (70)$$

Thus, the equation of motion for the superfluid order parameter $\bar{\Delta}(\mathbf{r}, t)$ is obtained from the \mathbf{p} -summation of the (12)-component of Eq. (69). In the resulting equation, the contribution coming from the last term in Eq. (69) vanishes. Since our stability analysis only needs the time evolution of $\bar{\Delta}(\mathbf{r}, t)$, the last term in Eq. (69) may be ignored for our purpose [62].

We also note that the first term on the right hand side in Eq. (69) represents the unitary time evolution. When we only retain this term and further assume a uniform superfluid $\bar{\Delta}(\mathbf{r}, t) = \bar{\Delta}(t)$, the QKE (69) is reduced to

$$i\partial_t \tilde{\mathcal{G}}_{\mathbf{p}}^{\leq}(t) = [\xi_{\mathbf{p}}\tau_3 - \bar{\Delta}(t), \tilde{\mathcal{G}}_{\mathbf{p}}^{\leq}(t)]. \quad (71)$$

This is equivalent to the so-called time-dependent Bogoliubov-de Gennes (TDBdG) equation [63, 64], which has widely been used in studying the dynamics of a closed Fermi condensate. In this sense, Eq. (69) may be interpreted as an extension of TDBdG theory to the open Fermi system shown in Fig. 1.

B. Stability analysis of non-equilibrium superfluid steady states

Using the QKE scheme discussed in Sec. III.A, we are now in the position to study the stability of the obtained steady states. We compute the time evolution of the superfluid order parameter $\bar{\Delta}(\mathbf{r}, t)$ in the situation where the initial condition is prepared arbitrarily close to the steady-state solution Δ_0 . We can then judge the stability of the solution by checking whether the deviation converges to zero or amplifies even more. It is useful to consider the deviation of the superfluid order parameter from the steady-state value:

$$\delta\bar{\Delta}(\mathbf{r}, t) = \bar{\Delta}(\mathbf{r}, t) - \Delta_0 = -iU \sum_{\mathbf{p}} \delta\tilde{\mathcal{G}}_{\mathbf{p}}^<(\mathbf{r}, t)_{12}, \quad (72)$$

Here, $\delta\tilde{\mathcal{G}}_{\mathbf{p}}^<(\mathbf{r}, t) \equiv \tilde{\mathcal{G}}_{\mathbf{p}}^<(\mathbf{r}, t) - \tilde{\mathcal{G}}_{\mathbf{p},\text{NESS}}^<$ is the deviation of the lesser Green's function from the (non-equilibrium) mean-field value, where

$$\tilde{\mathcal{G}}_{\mathbf{p},\text{NESS}}^< = \int \frac{d\omega}{2\pi} \tilde{\mathcal{G}}_{\mathbf{p},\text{NESS}}^<(\omega) \quad (73)$$

is the ω -integrated lesser Green's function in the non-equilibrium steady state, with $\tilde{\mathcal{G}}^<(\mathbf{p}, \omega)$ being given in Eq. (45). $\delta\bar{\Delta}(\mathbf{r}, t)$ decays (amplifies) as a function of time if the steady state solution is (un)stable.

To derive the equation for the dynamics of $\delta\bar{\Delta}(\mathbf{r}, t)$, it is useful to linearize the QKE (69) in terms of $\delta\bar{\Delta}(\mathbf{r}, t)$ and $\delta\tilde{\mathcal{G}}_{\mathbf{p}}^<(\mathbf{r}, t)$. Carrying out the Fourier transformation with respect to \mathbf{r} , one has

$$\begin{aligned} i\partial_t \delta\tilde{\mathcal{G}}_{\mathbf{p}}^<(\mathbf{q}, t) &= [\xi_{\mathbf{p}}\tau_3 - \tilde{\Delta}_0, \delta\tilde{\mathcal{G}}_{\mathbf{p}}^<(\mathbf{q}, t)]_- - [\delta\tilde{\Delta}(\mathbf{q}, t), \tilde{\mathcal{G}}_{\mathbf{p},\text{NESS}}^<]_- - \frac{Q^2 - q^2}{8m} [\tau_3, \delta\tilde{\mathcal{G}}_{\mathbf{p}}^<(\mathbf{q}, t)]_- \\ &+ \frac{\mathbf{p} \cdot \mathbf{q}}{2m} [\tau_3, \delta\tilde{\mathcal{G}}_{\mathbf{p}}^<(\mathbf{q}, t)]_+ + \frac{\mathbf{Q} \cdot \mathbf{q}}{4m} [\tau_0, \delta\tilde{\mathcal{G}}_{\mathbf{p}}^<(\mathbf{q}, t)]_+ - 4i\gamma \delta\tilde{\mathcal{G}}_{\mathbf{p}}^<(\mathbf{r}, t) - 4\gamma \int_{-\infty}^{\infty} \frac{d\omega}{2\pi} F(\omega) \delta\mathcal{A}(\mathbf{p}, \omega, \mathbf{q}, t), \end{aligned} \quad (74)$$

where $\tilde{\Delta}_0 = \Delta_0\tau_1$ and

$$\delta\tilde{\mathcal{G}}_{\mathbf{p}}^<(\mathbf{q}, t) = \int d\mathbf{r} e^{-i\mathbf{q} \cdot \mathbf{r}} \delta\tilde{\mathcal{G}}_{\mathbf{p}}^<(\mathbf{r}, t), \quad (75)$$

$$\delta\tilde{\Delta}(\mathbf{q}, t) = \int d\mathbf{r} e^{-i\mathbf{q} \cdot \mathbf{r}} \delta\tilde{\Delta}(\mathbf{r}, t) \equiv \delta\tilde{\Delta}(\mathbf{q}, t)\tau_+ + \delta\tilde{\Delta}^*(\mathbf{q}, t)\tau_-. \quad (76)$$

Here,

$$\delta\mathcal{A}(\mathbf{p}, \omega, \mathbf{q}, t) = \sum_{\eta=\pm} \left[\frac{4\gamma}{[\omega - \eta E_{\mathbf{p},\mathbf{Q}}^{0,\eta}]^2 + 4\gamma^2} \delta\Xi_{\mathbf{p},\mathbf{Q}}^{\eta}(\mathbf{q}, t) + \frac{8\gamma[\omega - \eta E_{\mathbf{p},\mathbf{Q}}^{0,\eta}]}{[[\omega - \eta E_{\mathbf{p},\mathbf{Q}}^{0,\eta}]^2 + 4\gamma^2]^2} \Xi_{\mathbf{p},\mathbf{Q}}^{0,\eta} \delta E_{\mathbf{p},\mathbf{Q}}(\mathbf{q}, t) \right] \quad (77)$$

is the linearized time-dependent spectral function, which is obtained by linearizing $\mathcal{A}(\mathbf{p}, \omega, \mathbf{r}, t)$ in Eq. (68) with respect to $\delta\bar{\Delta}(\mathbf{r}, t)$. We have also introduced here

$$\begin{aligned} \delta\Xi_{\mathbf{p},\mathbf{Q}}^+(\mathbf{q}, t) &= -\delta\Xi_{\mathbf{p},\mathbf{Q}}^-(\mathbf{q}, t) \\ &= -\frac{1}{2[E_{\mathbf{p},\mathbf{Q}}^0]^2} \begin{pmatrix} \xi_{\mathbf{p},\mathbf{Q}}^{(s)} \delta E_{\mathbf{p},\mathbf{Q}}(\mathbf{q}, t) & E_{\mathbf{p},\mathbf{Q}}^0 \delta\bar{\Delta}(\mathbf{q}, t) + \Delta_0 \delta E_{\mathbf{p},\mathbf{Q}}(\mathbf{q}, t) \\ E_{\mathbf{p},\mathbf{Q}}^0 \delta\bar{\Delta}^*(\mathbf{q}, t) + \Delta_0 \delta E_{\mathbf{p},\mathbf{Q}}(\mathbf{q}, t) & -\xi_{\mathbf{p},\mathbf{Q}}^{(s)} \delta E_{\mathbf{p},\mathbf{Q}}(\mathbf{q}, t) \end{pmatrix}, \end{aligned} \quad (78)$$

and

$$\delta E_{\mathbf{p},\mathbf{Q}}(\mathbf{q}, t) = \frac{\Delta_0}{E_{\mathbf{p},\mathbf{Q}}^0} \text{Re}[\delta\bar{\Delta}(\mathbf{q}, t)]. \quad (79)$$

Since Eq. (74) does not involve any mode-coupling term, one may safely focus on a particular value of the momentum \mathbf{q} ($\equiv \bar{\mathbf{q}}$) in considering how the initial deviation of the superfluid order parameter from the mean-field value evolves over time. Keeping this in mind, we take the following initial condition for the quantum kinetic equation (74):

$$\delta\bar{\Delta}(\bar{\mathbf{q}}, t = 0) = [\Delta_0 + \delta|\bar{\Delta}(\bar{\mathbf{q}}, t = 0)] e^{i\bar{\mathbf{q}} \cdot \mathbf{r}} - \Delta_0. \quad (80)$$

Here, $\delta|\bar{\Delta}(\bar{\mathbf{q}}, t = 0)|$ and $\bar{\mathbf{q}} \cdot \mathbf{r}$ physically have the meanings of amplitude and phase deviations from the mean-field value Δ_0 , respectively.

We numerically solve Eq. (74) in the weak-coupling regime $(p_F a_s)^{-1} = -1$, by using the fourth order implicit Runge-Kutta method with small time steps. At each time step, the deviation $\delta\bar{\Delta}(\bar{\mathbf{q}}, t)$ in the right-hand-side of this equation is evaluated from $\delta\tilde{\mathcal{G}}_p^<(\bar{\mathbf{q}}, t)$, to proceed to the next time step. Because our QKE approach uses the gradient expansion as explained in Sec. III A, we set the initial condition so as to satisfy $\delta|\bar{\Delta}(\bar{\mathbf{q}}, t = 0)| \ll \Delta_0$ and $|\bar{\mathbf{q}}| \ll p_F$ [65, 66].

IV. NON-EQUILIBRIUM SUPERFLUID STEADY STATES IN DRIVEN-DISSIPATIVE FERMION GAS

We now explore non-equilibrium superfluid steady states in a driven-dissipative Fermi gas. In Sec. IV.A, we first look for possible mean-field solutions of the gap equation (46), under the vanishing current condition in Eq. (48). As we have emphasized in the previous section, the solution of the gap equation (46) does not necessarily mean the stability of this pairing state. To assess which solutions are physical, we apply the stability analysis explained in Sec. III.B to each mean-field solution in Sec. IV.B.

A. Non-equilibrium superfluid steady states

Figure 4(a) summarizes the non-equilibrium superfluid steady state solutions of the gap equation (46) under the vanishing current condition in Eq. (48), in the weak-coupling regime $((p_F a_s)^{-1} = -1)$ of a driven-dissipative Fermi gas at $T_{\text{env}} = 0$ and $\gamma \rightarrow +0$. As seen in this figure, four self-consistent solutions are obtained under the ansatz in Eq. (28). Among them, NBCS (non-equilibrium BCS state) and NIG (non-equilibrium interior gap state) are isotropic superfluid states ($\mathbf{Q} = 0$). In particular, NBCS is reduced to the ordinary BCS state in the thermal equilibrium limit $\delta\mu \rightarrow 0$ (solid circle in Fig. 4(a)), so that it may be viewed as an extension of the ordinary BCS state to the non-equilibrium steady state. On the other hand, NIG is similar to the so-called interior gap state [67, 68] that arises in spin-imbalanced system, as we argue in the following. In the next subsection, we will show further that NBCS (NIG) is a (un)stable state, which is in parallel to the known results in equilibrium that the ordinary BCS state (interior gap state) is (un)stable against superfluid fluctuations (See Table I.). The remaining two solutions, NFF and NFF' (non-equilibrium Fulde-Ferrell states), are anisotropic superfluid state with $\mathbf{Q} \neq 0$. We briefly note that the existence of two kinds of FF states has also been pointed out in a thermal-equilibrium spin-imbalanced Fermi gas [55]. Actually, the former (latter) turns out to be a (un)stable state, as we will discuss in the next subsection, which is again parallel to the equilibrium case (See Table I.).

To grasp the character of each state, we conveniently

consider the pair amplitude,

$$P_{\mathbf{p}} \equiv \langle \bar{\psi}_{-\mathbf{p}, \downarrow}(t) \bar{\psi}_{\mathbf{p}, \uparrow}(t) \rangle, \quad (81)$$

which physically describes the pairing structure in momentum space. Here,

$$\bar{\psi}_{\mathbf{p}, \sigma}(t) = \int d\mathbf{r} e^{-i\mathbf{p} \cdot \mathbf{r}} \bar{\psi}_{\sigma}(\mathbf{r}, t) \quad (82)$$

is the Fourier transformation of the gauge-transformed field operator,

$$\bar{\psi}_{\sigma}(\mathbf{r}, t) = e^{-i\chi(\mathbf{r}, t)} \psi_{\sigma}(\mathbf{r}, t), \quad (83)$$

where the phase χ is given in Eq. (31). Within the present mean-field scheme, $P_{\mathbf{p}}$ in Eq. (81) can be evaluated from the lesser Green's function $\tilde{\mathcal{G}}^<(\mathbf{p}, \omega)$ in Eq. (45) as

$$\begin{aligned} P_{\mathbf{p}} &= -i \int \frac{d\omega}{2\pi} \tilde{\mathcal{G}}_{12}^<(\mathbf{p}, \omega) \\ &= -\frac{\Delta_0}{E_{\mathbf{p}, \mathbf{Q}}^0} \sum_{\eta=\pm} \eta \int \frac{d\omega}{2\pi} F(\omega) \frac{2\gamma}{[\omega - \eta E_{\mathbf{p}, \mathbf{Q}}^{0, \eta}]^2 + 4\gamma^2}. \end{aligned} \quad (84)$$

In the small damping limit $\gamma \rightarrow 0$ (which is the case of Fig. 4(a)), one may carry out the ω -integration in Eq. (84), giving

$$P_{\mathbf{p}} = \frac{\Delta_0}{2E_{\mathbf{p}, \mathbf{Q}}^0} \left[F(-E_{\mathbf{p}, \mathbf{Q}}^{0, -}) - F(E_{\mathbf{p}, \mathbf{Q}}^{0, +}) \right]. \quad (85)$$

In the NBCS and NIG cases ($\mathbf{Q} = 0$), Eq. (85) is reduced to

$$P_{\mathbf{p}} = \frac{\Delta_0}{2E_{\mathbf{p}}} [1 - 2F(E_{\mathbf{p}})], \quad (86)$$

where $E_{\mathbf{p}}$ is given below Eq. (47). In the thermal equilibrium BCS limit ($\delta\mu \rightarrow 0$), $F(E_{\mathbf{p}}) = f(E_{\mathbf{p}})$ vanishes at $T_{\text{env}} = 0$. Then, as well-known in the ordinary BCS theory, the pair amplitude,

$$P_{\mathbf{p}} = \frac{\Delta_0}{2\sqrt{(\varepsilon_{\mathbf{p}} - \mu)^2 + \Delta_0^2}}, \quad (87)$$

has large intensity around the Fermi momentum $p_F = \sqrt{2m\mu}$, indicating that Cooper pairs are dominantly formed around the Fermi surface. We also find from the definition of $F(\omega)$ in Eq. (44) that, even when $\delta\mu > 0$,

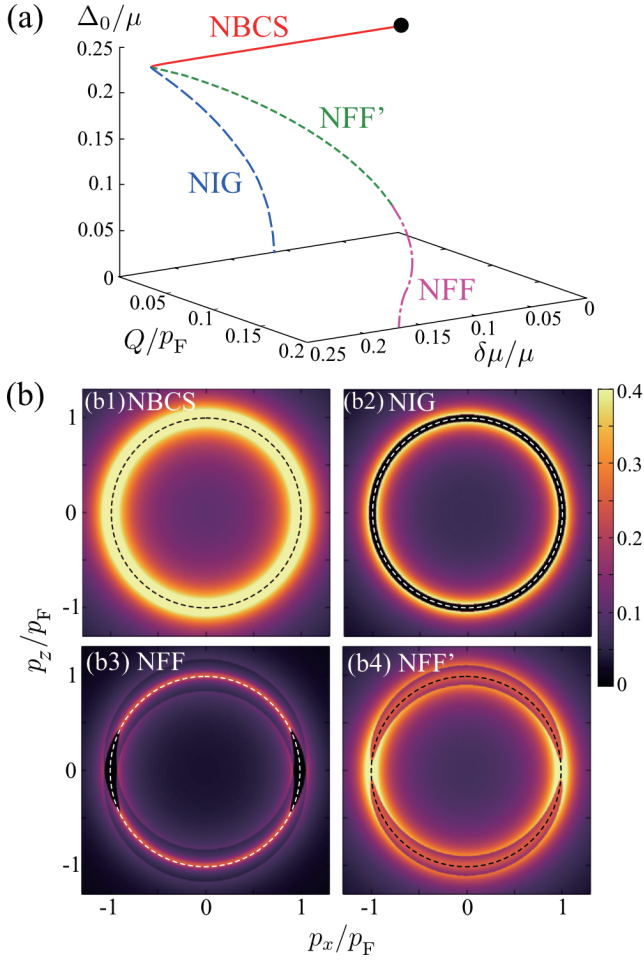


FIG. 4. (a) Non-equilibrium superfluid solutions of the gap equation (46) in the weak-coupling regime ($(p_F a_a)^{-1} = -1$) of a driven-dissipative Fermi gas. We set $T_{\text{env}} = 0$ and $\gamma \rightarrow +0$, and impose the vanishing current condition in Eq. (48). Among the four mean-field solutions, NBCS and NIG (non-equilibrium interior gap state) are uniform superfluid states ($\mathbf{Q} = 0$). NFF and NFF' are FF-like non-uniform states ($\mathbf{Q} \neq 0$ and $\mathbf{Q} \parallel p_z$). The solid circle is at the BCS state in the thermal equilibrium case ($\delta\mu = 0$). (b) Calculated intensity of the pair amplitude of each state, when $\delta\mu = 0.145\mu$. The dotted line in each panel shows the position at $p = p_F = \sqrt{2m\bar{\mu}}$. We will show in Sec. IV B that NBCS and NFF are stable solutions, while NIG and NFF' are unstable solutions.

Eq. (87) still holds, as far as $\Delta_0 \geq \delta\mu$. This is just the NBCS case. Indeed, as shown in Fig. 4(b1), the calculated NBCS pair amplitude has large intensity around $p_F = \sqrt{2m\bar{\mu}}$ (although p_F no longer has the meaning of the Fermi momentum, when $\delta\mu = 0.145\mu > 0$).

For NIG, although the pair amplitude $P_{\mathbf{p}}$ is also isotropic, it vanishes around the ‘‘Fermi momentum’’ $p = p_F$ (see Fig. 4(b2)). In this pairing state, the superfluid order parameter Δ_0 is not so large as the NBCS

case (see Fig. 4(a)). When $\Delta_0 < \delta\mu$, one obtains

$$P_{\mathbf{p}} = \frac{\Delta_0}{2\sqrt{(\varepsilon_{\mathbf{p}} - \mu)^2 + \Delta_0^2}} \Theta \left(\sqrt{(\varepsilon_{\mathbf{p}} - \mu)^2 + \Delta_0^2} - \delta\mu \right). \quad (88)$$

Equation (88) immediately explains the vanishing pairing amplitude around $p = p_F$ seen in Fig. 4(b2) (because the step function vanishes there). In addition, the region where $P_{\mathbf{p}} > 0$ is given by $p \leq \tilde{p}_{F1}$, $\tilde{p}_{F2} \leq p$, where

$$\tilde{p}_{F1} = \sqrt{2m \left[\mu - \sqrt{\delta\mu^2 - \Delta_0^2} \right]}, \quad (89)$$

$$\tilde{p}_{F2} = \sqrt{2m \left[\mu + \sqrt{\delta\mu^2 - \Delta_0^2} \right]}. \quad (90)$$

Particularly in the limiting case, $\delta\mu \gg \Delta_0$, one finds

$$\tilde{p}_{F1} \simeq \sqrt{2m[\mu - \delta\mu]} = p_{F1}, \quad (91)$$

$$\tilde{p}_{F2} \simeq \sqrt{2m[\mu + \delta\mu]} = p_{F2}, \quad (92)$$

that coincide with the positions of two edges imprinted on the Fermi momentum distribution $n_{\mathbf{p},\sigma}$ by the two reservoirs [39] (see Fig. 1). When we simply regard these edges as two ‘Fermi surfaces’ with different sizes, Fig. 4(b2) indicates that NIG Cooper pairs are formed around the ‘Fermi surfaces’ at p_{F1} and p_{F2} . This pairing structure is similar to the Sarma(-Liu-Wilczek) state [67, 68] (which is also referred to as the interior gap state in the literature) discussed in thermal equilibrium superconductivity under an external magnetic field, as well as in a spin imbalanced Fermi gas.

We next consider the anisotropic NFF and NFF' states with $\mathbf{Q} \neq 0$. To grasp their pairing structures, it is useful to rewrite Eq. (85) in the form,

$$P_{\mathbf{p}} = \frac{1}{2} [P_{\mathbf{p}}^{\text{FF}}(\mathbf{Q}, \delta\mu) + P_{-\mathbf{p}}^{\text{FF}}(\mathbf{Q}, -\delta\mu)], \quad (93)$$

where

$$P_{\mathbf{p}}^{\text{FF}}(\mathbf{Q}, \delta\mu) = \frac{\Delta_0}{2E_{\mathbf{p},\mathbf{Q}}^0} \left[1 - f(\bar{E}_{\mathbf{p},\mathbf{Q}}^+(\delta\mu)) - f(\bar{E}_{\mathbf{p},\mathbf{Q}}^-(\delta\mu)) \right]. \quad (94)$$

In Eq. (94), $\bar{E}_{\mathbf{p},\mathbf{Q}}^{\pm}(\delta\mu)$ is given in Eq. (42) where $\xi_{\pm\mathbf{p}+\mathbf{Q}/2}$ in $\xi_{\mathbf{p},\mathbf{Q}}^{(a)}$ is replaced by

$$\bar{\xi}_{\pm\mathbf{p}+\mathbf{Q}/2} = \varepsilon_{\pm\mathbf{p}+\mathbf{Q}/2} - \mu - \delta\mu. \quad (95)$$

Equation (94) is just the same form as the pair amplitude in the thermal equilibrium FF state [37, 38], when one regards $\delta\mu$ as an *external magnetic field*. Thus, the first (second) term in Eq. (93) may be viewed as the pair amplitude in the FF state under an external magnetic field $\delta\mu$ ($-\delta\mu$), which just corresponds to the pairing (A) ((B)) in Fig. 2(b).

In the thermal equilibrium FF state, when \mathbf{Q} points to the z direction, the pair amplitude is known to have large intensity around the Fermi surface in the region

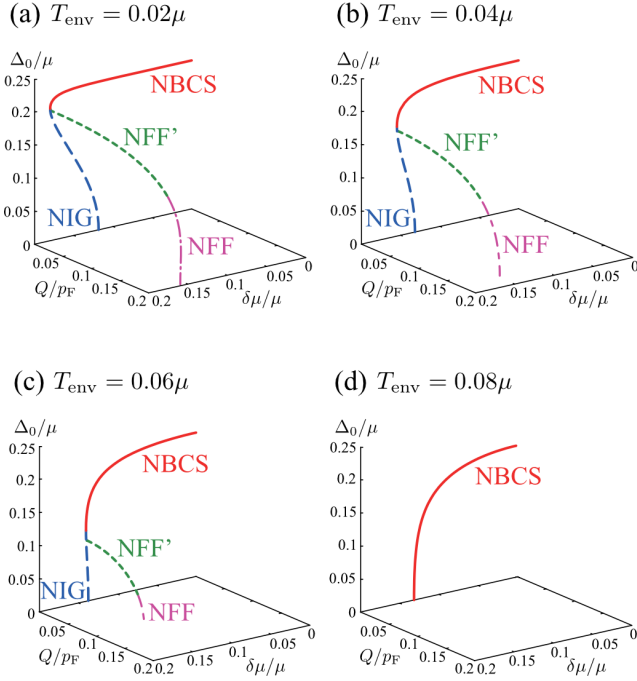


FIG. 5. Same plots as Fig. 4(a) for non-zero environment temperatures T_{env} .

$p_z > 0$ [37, 38]. Thus, in Figs. 4(b3) and (b4), the anisotropic pair amplitude in the upper-half (lower-half) plane is dominated by the first term $P_{\mathbf{p}}^{\text{FF}}(\mathbf{Q}, \delta\mu)$ (second term ($P_{-\mathbf{p}}^{\text{FF}}(\mathbf{Q}, -\delta\mu)$) in Eq. (93).

Because the two-edge structure of the Fermi momentum distribution $n_{\mathbf{p},\sigma}$ at p_{F1} and p_{F2} are essentially important in obtaining NIG, NFF, and NFF' solutions, these states are expected to be suppressed when this structure is blurred with increasing the environment temperature T_{env} . This can be confirmed in Fig. 5, where one sees that only the NBCS state remains at $T_{\text{env}} = 0.08\mu$. Of course, NBCS also eventually disappears at higher T_{env} as in the thermal equilibrium case, although we do not explicitly show the result here.

We note that, while the chemical potential difference $\delta\mu$ produces the two-edge structure p_{F1} and p_{F2} in $n_{\mathbf{p},\sigma}$, this structure may also be viewed as the smearing of the Fermi surface edge at $p_F = \sqrt{2m\mu}$. Because this is a similar effect to the thermal broadening, all the four solutions eventually disappear when $\delta\mu$ is large to some extent, as shown in Figs. 4(a) and 5. We also briefly note that the same depairing mechanism also works when the damping rate γ becomes large, because it also blurs the Fermi surface edge at p_F [39].

B. Stability analysis of non-equilibrium superfluid solutions

We next assess the stability of the four non-equilibrium superfluid solutions (NBCS, NIG, NFF, and NFF') ob-

TABLE I. Summary of the stability analysis for $T_{\text{env}} = 0$ and $\gamma = 0.005\mu$. Among the superfluid solutions, the underlined states are only stable.

region	superfluid solutions
region I ($0 < \delta\mu \leq 0.111\mu$)	<u>NBCS</u>
region II ($0.111\mu < \delta\mu \leq 0.135\mu$)	<u>NBCS</u> , <u>NIG</u>
region III ($0.135\mu < \delta\mu \leq 0.152\mu$)	<u>NBCS</u> , <u>NIG</u> , <u>NFF</u> , <u>NFF'</u>
region IV ($0.152\mu < \delta\mu \leq 0.183\mu$)	<u>NBCS</u> , <u>NIG</u> , <u>NFF'</u>

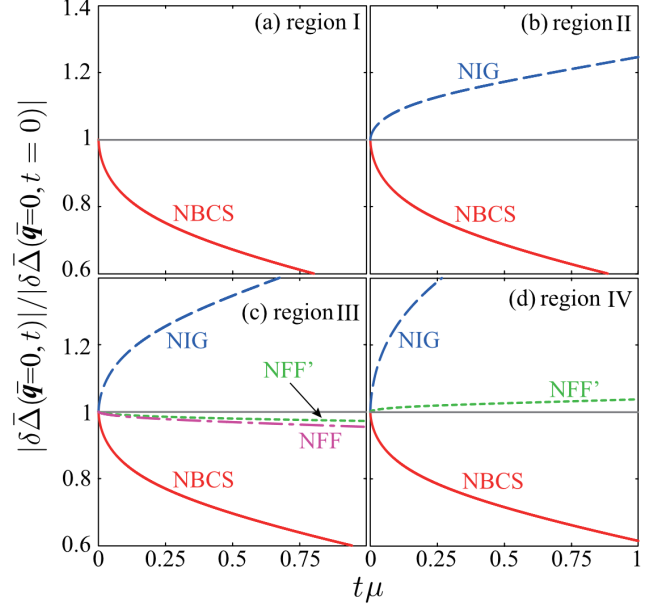


FIG. 6. Calculated time evolution of the deviation $|\delta\bar{\Delta}(\bar{\mathbf{q}} = 0, t)|$ of the superfluid order parameter from the mean-field value. We set $T_{\text{env}} = 0$, $\gamma = 0.005\mu$, and $|\delta\bar{\Delta}(\bar{\mathbf{q}} = 0, t = 0)| = 0.001\mu$. (a) $\delta\mu = 0.05\mu$ (region I). (b) $\delta\mu = 0.13\mu$ (region II). (c) $\delta\mu = 0.145\mu$ (region III). (d) $\delta\mu = 0.16\mu$ (region IV).

tained in Sec. IV.A, by solving the linearized quantum kinetic equation (74) under the initial condition in Eq. (80). Table I summarizes our result for $T_{\text{env}} = 0$ and $\gamma = 0.005\mu$. For finite bath temperature results, see also Fig. 2(a), which shows the same sets of the solution to be stable. We found that BCS and NFF are stable steady-state solutions in all regions, while NIG and NFF' are unstable.

We report below the stability analysis result that confirms these results. Figure 6 shows the time evolution of the deviations of the superfluid order parameter from the mean-field value, when the amplitude deviation is only considered at $t = 0$ ($\bar{\mathbf{q}} = 0$ and $|\delta\bar{\Delta}(\bar{\mathbf{q}} = 0, t = 0)| \neq 0$). In the NBCS case, we see in this figure that the deviation $|\delta\bar{\Delta}(\bar{\mathbf{q}} = 0)|$ decays over time in all the regions I-IV. This means that NBCS is stable against small perturbation in terms of the amplitude of the superfluid order parameter. The same conclusion is also obtained in the presence of phase deviation ($\bar{\mathbf{q}} \neq 0$). As an example, we show in Fig. 7(a) the result in the region III. Thus, we judge that

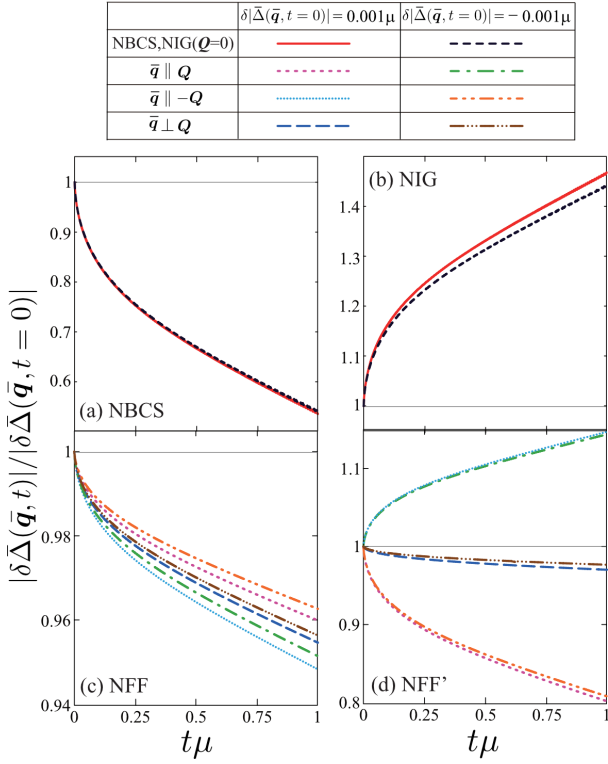


FIG. 7. Calculated time evolution of $|\delta\bar{\Delta}(\bar{q}, t)|$ in the region III ($\delta\mu = 0.145\mu$), when $|\bar{q}| = 0.001p_F > 0$. We take $T_{\text{env}} = 0$, $\gamma = 0.005\mu$. (a) NBCS. (b) NIG. (c) NFF. (d) NFF'. In this figure, “ $\bar{q} \parallel \pm\mathbf{Q}$ ” show the cases when \bar{q} is parallel and points to $\pm\mathbf{Q}$. Because NBCS and NIG are isotropic with $\mathbf{Q} = 0$, the results shown in panels (a) and (b) do not depend on the direction of \bar{q} .

NBCS is a *stable* non-equilibrium superfluid steady state.

In contrast to NBCS, NIG exhibits the opposite behavior, as seen in Figs. 6(b)-(d): The deviation $|\delta\bar{\Delta}(\bar{q} = 0, t)|$ grows over time, indicating that, although NIG is one of the four mean-field solutions, it is actually destroyed by this small perturbation. The instability of this state is also seen when $\bar{q} \neq 0$, as shown in Fig. 7(b). These results conclude that NIG is *unstable*.

For the anisotropic solutions with $\mathbf{Q} \neq 0$, Figs. 6(c) and 7(c) conclude that NFF is a *stable* FF-type superfluid state in the region III. For NFF', as far as the perturbation with $\bar{q} = 0$ is considered, while it is unstable in the region IV, it is stable in the region III (see Figs. 6(d) and (c), respectively). However, even in the latter region, Fig. 7(d) shows that this FF-type state cannot be always stable against the initial deviation with $\bar{q} \neq 0$. In this sense, we classify NFF' as an *unstable* superfluid state.

The above conclusions hold true even in the case with finite bath temperature $T_{\text{env}} > 0$ and $\gamma > 0$: We show in Fig. 8 effects of the environment temperature T_{env} (panel (a)) and damping rate γ (panel (b)) on the time evolution of $|\delta\bar{\Delta}(\bar{q} = 0, t)|$ in the NBCS case: Initial deviations is found to always decay over time, irrespective of the values

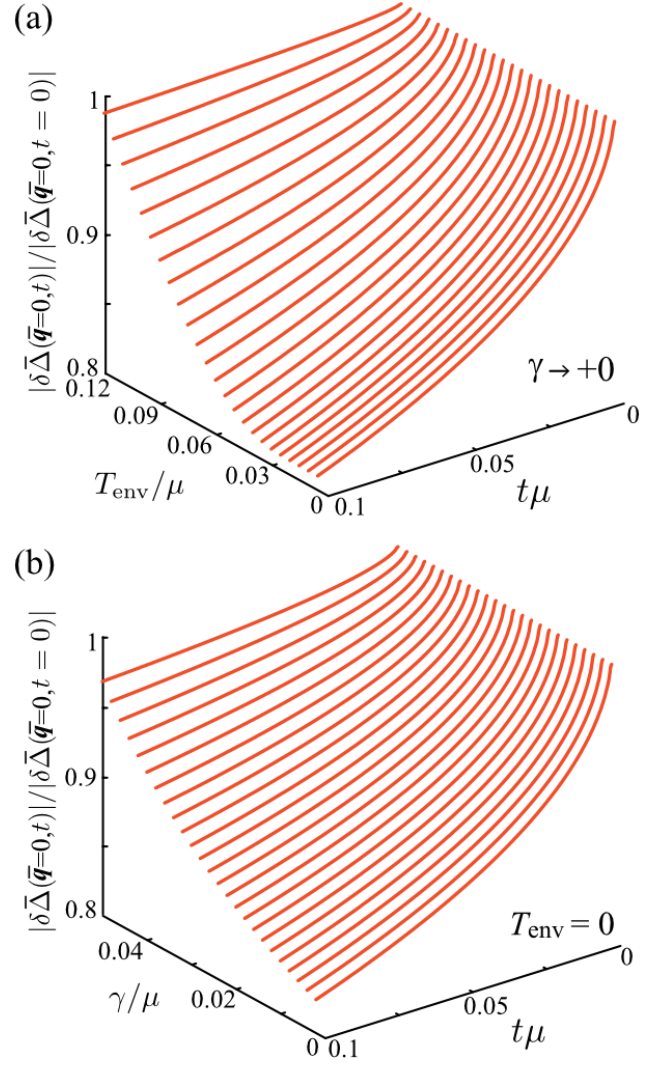


FIG. 8. Time evolution of the deviation $|\delta\bar{\Delta}(\bar{q} = 0, t)|$ from the NBCS mean-field order parameter and effects of (a) environment temperature T_{env} , and (b) damping rate γ . We take $\delta\mu = 0.05\mu$, and $|\delta\bar{\Delta}(\bar{q} = 0, t=0)| = 0.001\mu$. In panels (a) and (b), we set $\gamma \rightarrow +0$ and $T_{\text{env}} = 0$, respectively.

of these environment parameters.

We also find from Fig. 8 that the relaxation time (time scale to recover the mean-field solution) depends on the environment parameters, T_{env} and γ . For the damping rate γ , because it is related to the system-reservoir coupling Λ (see Eq. (27)), we find from Fig. 8(b) that small coupling strengths would be preferable for this purpose.

Summarizing the above-mentioned stability analyses for various parameter sets $(T_{\text{env}}, \gamma, \delta\mu)$, we obtain the phase diagram in Fig. 2(a). Among the four candidates (NBCS, NIG, NFF, NFF'), NBCS and NFF only survive as stable non-equilibrium superfluid steady states. In the superfluid region, NBCS is always stable. Thus, in the region where NFF is stable, the bistability occurs. We also see in Fig. 2(a) the existence of the other bistability region where NBCS and the normal state are both stable.

Because the energetic consideration, which is useful in determining the *thermodynamically stable state*, does not work in the present non-equilibrium case, one cannot immediately identify which state is realized in the bistability region. As pointed out in Ref. [33], the answer to this question is considered to depend on how to tune the environment parameters. We also note that Refs. [69–71] clarify that a voltage-driven superconductor (where the momentum distribution of conduction electrons is highly non-thermal and exhibits a two-step structure as in the non-equilibrium case we are considering in this paper) shows the same kind of bistability, although the possibility of FF-like state has not been discussed. Our result is consistent with these previous work, and NEFF predicted in this paper would also be expected in such a voltage-driven superconductor.

V. SUMMARY

To summarize, we have discussed non-equilibrium superfluid steady states and their stability in a driven-dissipative Fermi gas. Using the Nambu-Keldysh Green's function technique, we extended the BCS theory developed in the thermal equilibrium state to the non-equilibrium steady state. To examine the stability of steady-state solutions obtained from this non-equilibrium BCS scheme, we also derived a quantum kinetic equation, to examine the time evolution of the superfluid order parameter.

By solving the non-equilibrium gap equation, we obtained four superfluid steady-state solutions: Among them, one of them (NBCS state) may be viewed as an extension of the ordinary thermal equilibrium BCS state to the non-equilibrium case, and another one (NIG state) is similar to the Sarma(-Liu-Wilczek) interior gap state. While these are isotropic uniform states, the remaining two are Fulde-Ferrell (FF) like anisotropic and non-uniform superfluid states (NFF and NFF' state), even though the present system has no spin imbalance. Analyzing their pair amplitudes, we found that the latter three superfluid solutions originate from the two-edge structure of the non-equilibrium Fermi momentum distribution which is produced by the coupled two reservoirs

with different chemical potentials. We also pointed out that each FF-like state may be viewed as the superposition of the thermal equilibrium FF state under an external magnetic field $h = \delta\mu$ and that under an external magnetic field $h = -\delta\mu$.

We then studied the stability of these four superfluid steady-state solutions, by solving the linearized quantum kinetic equation. This concluded that only the BCS-type state (NBCS) and one of the two FF-type states (NFF) are stable, in the sense that the initial deviation of the superfluid order parameter always decays over time. The other two, NIG and NFF', are unstable because small perturbation are amplified over time. These stability analyses lead to the phase diagram of a driven-dissipative Fermi gas shown in Fig. 2(a).

Our proposed Fermi-surface reservoir-engineering can be applied not only to the Fermi gas system but also to various many-body Fermi systems. Particularly in lattice systems, the combination of the band structure and multi-step structure on the Fermi momentum distribution may trigger unconventional ordered phases, such as spin- and charge-density wave-like states. The stability of such unconventional ordered phases can be assessed by evaluating the time evolution of fluctuations around steady-state value, in the same manner as this paper. The search for unconventional ordered phases in non-equilibrium systems is currently one of the most exciting challenges in the condensed matter physics, and our results would contribute to the further development of this research field.

ACKNOWLEDGMENTS

We thank D. Kagamihara and K. Furutani for discussions. T.K. was supported by MEXT and JSPS KAKENHI Grant-in-Aid for JSPS fellows Grant No.JP21J22452. R.H. was supported by an appointment to the JRG Program at the APCTP through the Science and Technology Promotion Fund and Lottery Fund of the Korean Government. Y.O. was supported by a Grant-in-aid for Scientific Research from MEXT and JSPS in Japan (No.JP18K11345, No.JP18H05406, and No.JP19K03689).

Appendix A: Derivation of Eq. (53)

We first introduce two inverse Green's functions $\overrightarrow{\mathcal{G}}_0^{-1}(1)$ and $\overleftarrow{\mathcal{G}}_0^{-1}(2)$, that obey

$$\overrightarrow{\mathcal{G}}_0^{-1}(1)\mathcal{G}_0^{\text{R(A)}}(1,2) = \delta(1-2)\tau_0, \quad (\text{A1})$$

$$\mathcal{G}_0^{\text{R(A)}}(1,2)\overleftarrow{\mathcal{G}}_0^{-1}(2) = \delta(1-2)\tau_0, \quad (\text{A2})$$

where $\mathcal{G}_0^{\text{R(A)}}(1,2)$ is the retarded (R) or advanced (A) component of the bare Green's function in Eq. (17), $\delta(1-2) = \delta(\mathbf{r}_1 - \mathbf{r}_2)\delta(t_1 - t_2)$, and the left (right) arrow on each differential operator means that it acts on the left (right) side

of this operator. From the Heisenberg equation of the field operator, these inverse Green's functions are found to have the forms,

$$\vec{\mathcal{G}}_0^{-1}(1) = \begin{pmatrix} i\vec{\partial}_{t_1} - h_0(-i\vec{\nabla}_{\mathbf{r}_1}) & 0 \\ 0 & i\vec{\partial}_{t_1} - h_0(-i\vec{\nabla}_{\mathbf{r}_1}) \end{pmatrix}, \quad (\text{A3})$$

$$\overleftarrow{\mathcal{G}}_0^{-1}(2) = \begin{pmatrix} -i\overleftarrow{\partial}_{t_2} - h_0(i\overleftarrow{\nabla}_{\mathbf{r}_2}) & 0 \\ 0 & -i\overleftarrow{\partial}_{t_2} - h_0(i\overleftarrow{\nabla}_{\mathbf{r}_2}) \end{pmatrix}, \quad (\text{A4})$$

where $h_0(-i\nabla_{\mathbf{r}}) = (-i\nabla_{\mathbf{r}})^2/(2m)$. Carrying out the gauge transformation discussed in Eqs. (29)-(31), one has

$$\begin{aligned} \vec{\mathcal{G}}_0^{-1}(1) &\equiv e^{-i\chi(1)\tau_3} \vec{\mathcal{G}}_0^{-1}(1) e^{i\chi(1)\tau_3} \\ &= \begin{pmatrix} i\vec{\partial}_{t_1} - h_0(-i\vec{\nabla}_{\mathbf{r}_1} + \mathbf{Q}/2) + \mu & 0 \\ 0 & i\vec{\partial}_{t_1} + h_0(-i\vec{\nabla}_{\mathbf{r}_1} + \mathbf{Q}/2) + \mu \end{pmatrix}, \end{aligned} \quad (\text{A5})$$

$$\begin{aligned} \overleftarrow{\mathcal{G}}_0^{-1}(2) &\equiv e^{-i\chi(2)\tau_3} \overleftarrow{\mathcal{G}}_0^{-1}(2) e^{-i\chi(2)\tau_3} \\ &= \begin{pmatrix} -i\overleftarrow{\partial}_{t_2} - h_0(i\overleftarrow{\nabla}_{\mathbf{r}_2} + \mathbf{Q}/2) + \mu & 0 \\ 0 & -i\overleftarrow{\partial}_{t_2} + h_0(i\overleftarrow{\nabla}_{\mathbf{r}_2} + \mathbf{Q}/2) + \mu \end{pmatrix}. \end{aligned} \quad (\text{A6})$$

Operating $\vec{\mathcal{G}}_0^{-1}(1)$ and $\overleftarrow{\mathcal{G}}_0^{-1}(2)$ to the Dyson equation of the (gauge transformed) lesser Green's function [48, 49],

$$\tilde{\mathcal{G}}^<(1, 2) = [\tilde{\mathcal{G}}^{\text{R}} \circ \tilde{\Sigma}^< \circ \tilde{\mathcal{G}}^{\text{A}}](1, 2), \quad (\text{A7})$$

from the left and the right, we have, respectively,

$$\vec{\mathcal{G}}_0^{-1}(1)\tilde{\mathcal{G}}^<(1, 2) = [\tilde{\Sigma}^< \circ \tilde{\mathcal{G}}^{\text{A}} + \tilde{\Sigma}^{\text{R}} \circ \tilde{\mathcal{G}}^<](1, 2), \quad (\text{A8})$$

$$\tilde{\mathcal{G}}^<(1, 2)\overleftarrow{\mathcal{G}}_0^{-1}(2) = [\tilde{\mathcal{G}}^{\text{R}} \circ \tilde{\Sigma}^< + \tilde{\mathcal{G}}^< \circ \tilde{\Sigma}^{\text{A}}](1, 2). \quad (\text{A9})$$

In obtaining these equations, we have used

$$\vec{\mathcal{G}}_0^{-1}(1)\tilde{\mathcal{G}}^{\text{R(A)}}(1, 2) = \delta(1-2)\tau_0 + [\tilde{\Sigma}^{\text{R(A)}} \circ \tilde{\mathcal{G}}^{\text{R(A)}}](1, 2), \quad (\text{A10})$$

$$\tilde{\mathcal{G}}^{\text{R(A)}}(1, 2)\overleftarrow{\mathcal{G}}_0^{-1}(2) = \delta(1-2)\tau_0 + [\tilde{\mathcal{G}}^{\text{R(A)}} \circ \tilde{\Sigma}^{\text{R(A)}}](1, 2). \quad (\text{A11})$$

Equations (A8) and (A9) yield the Kadanoff-Baym (KB) equation [48, 61],

$$[\vec{\mathcal{G}}_0^{-1}\tilde{\mathcal{G}}^< - \tilde{\mathcal{G}}^<\overleftarrow{\mathcal{G}}_0^{-1}](1, 2) = [\tilde{\Sigma}^{\text{R}} \circ \tilde{\mathcal{G}}^< - \tilde{\mathcal{G}}^< \circ \tilde{\Sigma}^{\text{A}} + \tilde{\Sigma}^< \circ \tilde{\mathcal{G}}^{\text{A}} - \tilde{\mathcal{G}}^{\text{R}} \circ \tilde{\Sigma}^<](1, 2). \quad (\text{A12})$$

Carrying out the Wigner transformation, which is followed by the ω -integration, one finds that the KB equation (A12) becomes

$$\vec{\mathcal{G}}_0^{-1}\tilde{\mathcal{G}}_{\mathbf{p}}^<(\mathbf{r}, t) - \tilde{\mathcal{G}}_{\mathbf{p}}^<(\mathbf{r}, t)\overleftarrow{\mathcal{G}}_0^{-1} = \mathcal{I}_{\mathbf{p}}(\mathbf{r}, t), \quad (\text{A13})$$

where $\mathcal{I}_{\mathbf{p}}(\mathbf{r}, t)$ is given in the sum of Eqs. (54) and (55). Since the left hand side of Eq. (A13) is evaluated as

$$\begin{aligned} \vec{\mathcal{G}}_0^{-1}\tilde{\mathcal{G}}_{\mathbf{p}}^<(\mathbf{r}, t) - \tilde{\mathcal{G}}_{\mathbf{p}}^<(\mathbf{r}, t)\overleftarrow{\mathcal{G}}_0^{-1} &= i\partial_t\tilde{\mathcal{G}}_{\mathbf{p}}^<(\mathbf{r}, t) - [\xi_{\mathbf{p}}\tau_3, \tilde{\mathcal{G}}_{\mathbf{p}}^<(\mathbf{r}, t)]_- - \left[\frac{\mathbf{Q}^2}{8m}\tau_3, \tilde{\mathcal{G}}_{\mathbf{p}}^<(\mathbf{r}, t) \right]_- \\ &+ \left[\frac{1}{8m}\tau_3, \nabla_{\mathbf{r}}^2\tilde{\mathcal{G}}_{\mathbf{p}}^<(\mathbf{r}, t) \right]_- + \frac{i}{2} \left[\frac{\mathbf{p}}{m}\tau_3, \nabla_{\mathbf{r}}\tilde{\mathcal{G}}_{\mathbf{p}}^<(\mathbf{r}, t) \right]_+ + \frac{i}{2} \left[\frac{\mathbf{Q}}{2m}\tau_0, \nabla_{\mathbf{r}}\tilde{\mathcal{G}}_{\mathbf{p}}^<(\mathbf{r}, t) \right]_+, \end{aligned} \quad (\text{A14})$$

one reaches Eq. (53).

Appendix B: Vanishment of the last term in Eq. (64)

To evaluate $\mathcal{R}(\mathbf{p}, \omega, \mathbf{r}, t)$ in Eq. (66), we carry out the Wigner transformation of Eqs. (A10) and (A11). Then, retaining the Moyal product to the first-order gradient expansion explained below Eq. (56), we have

$$\begin{aligned} \vec{\mathcal{G}}_0^{-1} \tilde{\mathcal{G}}^{\text{R(A)}}(\mathbf{p}, \omega, \mathbf{r}, t) &= \tau_0 + [\tilde{\Sigma}^{\text{R(A)}} \circ \tilde{\mathcal{G}}^{\text{R(A)}}](\mathbf{p}, \omega, \mathbf{r}, t) \\ &\simeq \tau_0 + \tilde{\Sigma}^{\text{R(A)}}(\mathbf{p}, \omega, \mathbf{r}, t) \tilde{\mathcal{G}}^{\text{R(A)}}(\mathbf{p}, \omega, \mathbf{r}, t), \end{aligned} \quad (\text{B1})$$

$$\begin{aligned} \tilde{\mathcal{G}}^{\text{R(A)}} \overleftarrow{\mathcal{G}}_0^{-1}(\mathbf{p}, \omega, \mathbf{r}, t) &= \tau_0 + [\tilde{\mathcal{G}}^{\text{R(A)}} \circ \tilde{\Sigma}^{\text{R(A)}}](\mathbf{p}, \omega, \mathbf{r}, t) \\ &\simeq \tau_0 + \tilde{\mathcal{G}}^{\text{R(A)}}(\mathbf{p}, \omega, \mathbf{r}, t) \tilde{\Sigma}^{\text{R(A)}}(\mathbf{p}, \omega, \mathbf{r}, t). \end{aligned} \quad (\text{B2})$$

The sum of these equations gives

$$\left[\omega \tau_0 - \xi_{\mathbf{p}} \tau_3 - \frac{\mathbf{Q}^2}{8m} \tau_3 - \frac{1}{2} \frac{\mathbf{p}}{m} \cdot \mathbf{Q} \tau_0 - \tilde{\Sigma}^{\text{R(A)}}(\mathbf{p}, \omega, \mathbf{r}, t), \tilde{\mathcal{G}}^{\text{R(A)}}(\mathbf{p}, \omega, \mathbf{r}, t) \right]_+ = 2\tau_0. \quad (\text{B3})$$

Here, $\tilde{\Sigma}^{\text{R(A)}}(\mathbf{p}, \omega, \mathbf{r}, t) = \tilde{\Sigma}_{\text{int}}^{\text{R(A)}}(\mathbf{p}, \omega, \mathbf{r}, t) + \tilde{\Sigma}_{\text{env}}^{\text{R(A)}}(\mathbf{p}, \omega, \mathbf{r}, t)$. This equation yields

$$\tilde{\mathcal{G}}^{\text{R}}(\mathbf{p}, \omega, \mathbf{r}, t) = \sum_{\eta=\pm} \frac{1}{\omega + 2i\gamma - E_{\mathbf{p}, \mathbf{Q}}^{\eta}(\mathbf{r}, t)} \Xi_{\mathbf{p}, \mathbf{Q}}^{\eta}(\mathbf{r}, t), \quad (\text{B4})$$

$$\tilde{\mathcal{G}}^{\text{A}}(\mathbf{p}, \omega, \mathbf{r}, t) = \sum_{\eta=\pm} \frac{1}{\omega - 2i\gamma - E_{\mathbf{p}, \mathbf{Q}}^{\eta}(\mathbf{r}, t)} \Xi_{\mathbf{p}, \mathbf{Q}}^{\eta}(\mathbf{r}, t), \quad (\text{B5})$$

where

$$E_{\mathbf{p}, \mathbf{Q}}^{\pm}(\mathbf{r}, t) = \sqrt{(\xi_{\mathbf{p}, \mathbf{Q}}^{(\text{s})})^2 + |\tilde{\Delta}(\mathbf{r}, t)|^2} \pm \xi_{\mathbf{p}, \mathbf{Q}}^{\text{a}} \equiv E_{\mathbf{p}, \mathbf{Q}}(\mathbf{r}, t) \pm \xi_{\mathbf{p}, \mathbf{Q}}^{(\text{a})}, \quad (\text{B6})$$

$$\Xi_{\mathbf{p}, \mathbf{Q}}^{\pm} = \frac{1}{2} \left[\tau_0 \pm \frac{\xi_{\mathbf{p}, \mathbf{Q}}^{(\text{s})}}{E_{\mathbf{p}, \mathbf{Q}}(\mathbf{r}, t)} \tau_3 \mp \frac{\tilde{\Delta}(\mathbf{r}, t)}{E_{\mathbf{p}, \mathbf{Q}}(\mathbf{r}, t)} \right]. \quad (\text{B7})$$

Equation (B4) may be viewed an extension of the Green's function in the non-equilibrium steady state in Eq. (39) to the case when the superfluid order parameter $\tilde{\Delta}(\mathbf{r}, t)$ depends on t and \mathbf{r} as given in Eq. (52).

Subtracting Eqs. (B1) from (B2), one obtains

$$i\partial_t \tilde{\mathcal{G}}^{\text{R(A)}}(\mathbf{p}, \omega, \mathbf{r}, t) = \left[\xi_{\mathbf{p}} \tau_3 + \frac{\mathbf{Q}^2}{8m} \tau_3 + \tilde{\Sigma}^{\text{R(A)}}(\mathbf{p}, \omega, \mathbf{r}, t), \tilde{\mathcal{G}}^{\text{R(A)}}(\mathbf{p}, \omega, \mathbf{r}, t) \right]. \quad (\text{B8})$$

Because $\tilde{\mathcal{G}}^{\text{R}}(\mathbf{p}, \omega, \mathbf{r}, t)$ and $\tilde{\mathcal{G}}^{\text{A}}(\mathbf{p}, \omega, \mathbf{r}, t)$ are, respectively, given by Eqs. (B4) and (B5), the right hand side of Eq. (B8) is found to vanish, which immediately proves $\partial_t \mathcal{R}(\mathbf{p}, \omega, \mathbf{r}, t) = 0$ in the last term in Eq. (64).

- | | |
|----------------------------------------------------------------------------------------------------------------------------------------------------------------------------------------------------------------------------------------------------------------------------------------------------------------------------------------------------------------------------------------------------------------------------------------------------------------------------------------------------------------------|---------------------------------------------------------------------------------------------------------------------------------------------------------------------------------------------------------------------------------------------------------------------------------------------------------------------------------------------------------------------------------------------------------------------------------------------------------------------------------------------------------------------------------------------------------------------------------|
| <p>[1] M. C. Marchetti, J. F. Joanny, S. Ramaswamy, T. B. Liverpool, J. Prost, M. Rao, and R. A. Simha, <i>Rev. Mod. Phys.</i> 85, 1143 (2013).</p> <p>[2] I. Carusotto and C. Ciuti, <i>Rev. Mod. Phys.</i> 85, 299 (2013).</p> <p>[3] L. M. Sieberer, M. Buchhold, and S. Diehl, <i>Rep. Prog. Phys.</i> 79, 096001 (2016).</p> <p>[4] Y. Ashida, Z. Gong, and M. Ueda, <i>Adv. Phys.</i> 69, 249 (2020).</p> <p>[5] M. Bukov, L. D'Alessio, and A. Polkovnikov, <i>Adv. Phys.</i></p> | <p>64, 139 (2015).</p> <p>[6] A. Eckardt, <i>Rev. Mod. Phys.</i> 89, 011004 (2017).</p> <p>[7] T. Oka and S. Kitamura, <i>Annu. Rev. Cond. Mat. Phys.</i> 10, 387 (2019).</p> <p>[8] F. Harper, R. Roy, M. S. Rudner, and S. Sondhi, <i>Annu. Rev. Condens. Matter Phys.</i> 11, 345 (2020).</p> <p>[9] H. Aoki, N. Tsuji, M. Eckstein, M. Kollar, T. Oka, and P. Werner, <i>Rev. Mod. Phys.</i> 86, 779 (2014).</p> <p>[10] V. Khemani, A. Lazarides, R. Moessner, and S. L. Sondhi, <i>Phys. Rev. Lett.</i> 116, 250401 (2016).</p> |
|----------------------------------------------------------------------------------------------------------------------------------------------------------------------------------------------------------------------------------------------------------------------------------------------------------------------------------------------------------------------------------------------------------------------------------------------------------------------------------------------------------------------|---------------------------------------------------------------------------------------------------------------------------------------------------------------------------------------------------------------------------------------------------------------------------------------------------------------------------------------------------------------------------------------------------------------------------------------------------------------------------------------------------------------------------------------------------------------------------------|

- [11] D. V. Else, B. Bauer, and C. Nayak, Phys. Rev. Lett. **117**, 090402 (2016).
- [12] N. Yao, A. C. Potter, I.-D. Potirniche, and A. Vishwanath, Phys. Rev. Lett. **118**, 030401 (2017), see also erratum.
- [13] D. V. Else, B. Bauer, and C. Nayak, Phys. Rev. X **7**, 011026 (2017).
- [14] J. Zhang, P. W. Hess, A. Kyprianidis, P. Becker, A. Lee, J. Smith, G. Pagano, I.-D. Potirniche, A.C. Potter, A. Vishwanath, N. Y. Yao, and C. Monroe, Nature (London) **543**, 217 (2017).
- [15] S. Choi, J. Choi, R. Landig, G. Kucsko, H. Zhou, J. Isoya, F. Jelezko, S. Onoda, H. Sumiya, V. Khemani, C. von Keyserlingk, N. Y. Yao, E. Demler, and M. D. Lukin, Nature (London) **543**, 221 (2017).
- [16] D. Fausti, R. I. Tobey, N. Dean, S. Kaiser, A. Dienst, M. C. Hoffmann, S. Pyon, T. Takayama, H. Takagi, and A. Cavalleri, Science **331**, 189 (2011).
- [17] M. Mitrano, A. Cantaluppi, D. Nicoletti, S. Kaiser, A. Perucchi, S. Lupi, P. Di Pietro, D. Pontiroli, M. Ricc3, S. R. Clark, D. Jaksch, and A. Cavalleri, Nature (London) **530**, 461 (2016).
- [18] T. Suzuki, T. Someya, T. Hashimoto, S. Michimae, M. Watanabe, M. Fujisawa, T. Kanai, N. Ishii, J. Itatani, S. Kasahara, Y. Matsuda, T. Shibauchi, K. Okazaki, and S. Shin, Commun. Phys. **2**, 115 (2019).
- [19] T. Vicsek, A. Czir3k, E. Ben-Jacob, I. Cohen, and O. Shochet, Phys. Rev. Lett. **75**, 1226 (1995).
- [20] J. Toner and Y. Tu, Phys. Rev. Lett. **75**, 4326 (1995).
- [21] M. Fruchart, R. Hanai, P. B. Littlewood, and V. Vitelli, Nature **592** 363 (2021).
- [22] R. Hanai and P. B. Littlewood, Phys. Rev. Res. **2**, 033018 (2020).
- [23] R. Hanai, A. Edelman, Y. Ohashi, and P. B. Littlewood, Phys. Rev. Lett. **122**, 185301 (2019). (2019).
- [24] Z. You, A. Baskaran, and M. C. Marchetti, Proc. Natl. Acad. Sci. U. S. A. **117**, 19767 (2020).
- [25] S. Saha, J. Agudo-Canalejo, and R. Golestanian, Phys. Rev. X **10**, 041009 (2020).
- [26] S. Diehl, A. Micheli, A. Kantian, B. Kraus, H. P. B3chler, and P. Zoller, Nature Phys. **4**, 878 (2008).
- [27] F. Verstraete, M. M. Wolf, and J. I. Cirac, Nat. Phys. **5**, 633 (2009).
- [28] H. Weimer, M. M3ller, I. Lesanovsky, P. Zoller, and H. P. B3chler, Nat. Phys. **6**, 382 (2010).
- [29] S. Diehl, E. Rico, M. A. Baranov, and P. Zoller, Nat. Phys. **7**, 971 (2011).
- [30] A. Metelmann and A. A. Clerk, Phys. Rev. X **5**, 021025 (2015).
- [31] R. Ma, B. Saxberg, C. Owens, N. Leung, Y. Lu, J. Simon, and D. I. Schuster, Nature (London) **566**, 51 (2019).
- [32] L. W. Clark, N. Schine, C. Baum, N. Jia, and J. Simon, Nature **582**, 41 (2020).
- [33] T. Kawamura, R. Hanai, and Y. Ohashi, companion paper, arXiv:2111.01385.
- [34] We note that the temperature cannot be defined in the main system, when it is out of equilibrium. In the thermal equilibrium limit, the system temperature coincides with the environment temperature T_{env} . In this paper, the term ‘temperature’ also means T_{env} in the thermally equilibrium reservoirs.
- [35] P. Fulde and R. A. Ferrell, Phys. Rev. **135**, A550 (1964).
- [36] A. I. Larkin and Y. N. Ovchinnikov, Zh. Eksp. Teor. Fiz. **47**, 1136 (1964) [Sov. Phys. JETP **20**, 762 (1965)].
- [37] S. Takada and T. Izuyama, Prog. Theor. Phys. **41**, 635 (1969).
- [38] H. Shimahara, Phys. Rev. B **50**, 12760 (1994).
- [39] T. Kawamura, R. Hanai, D. Kagamihara, D. Inotani, Y. Ohashi, Phys. Rev. A **101**, 013602 (2020).
- [40] Y. Nambu, Phys. Rev. **117**, 648 (1960).
- [41] J. R. Schrieffer, *Theory of Superconductivity* (Addison-Wesley, NY, 1964).
- [42] M. Randeria, in *Bose-Einstein Condensation*, edited by A. Griffin, D. W. Snoke, and S. Stringari (Cambridge University Press, Cambridge, UK, 1995), pp. 355-392.
- [43] R. Hanai, P. B. Littlewood, and Y. Ohashi, J. Low Temp. Phys. **183**, 127 (2016).
- [44] R. Hanai, P. B. Littlewood, and Y. Ohashi, Phys. Rev. B **96**, 125206 (2017).
- [45] R. Hanai, P. B. Littlewood, and Y. Ohashi, Phys. Rev. B **97**, 245302 (2018).
- [46] J. C. Cuevas, A. Mart3n-Rodero, and A. Levy Yeyati, Phys. Rev. B **54**, 7366 (1996).
- [47] T. Kawamura, D. Kagamihara, R. Hanai, and Y. Ohashi, J. Low Temp. Phys. **201**, 41-48 (2020).
- [48] J. Rammer, *Quantum Field Theory of Non-equilibrium States* (Cambridge University Press, Cambridge, 2007).
- [49] A. Zagoskin, *Quantum Theory of Many-Body Systems* (Springer, New York, 2014).
- [50] M. H. Szymańska, J. Keeling, and P. B. Littlewood, Phys. Rev. Lett. **96**, 230602 (2006).
- [51] M. Yamaguchi, K. Kamide, T. Ogawa, and Y. Yamamoto, New J. Phys. **14**, 065001 (2012).
- [52] M. Yamaguchi, R. Nii, K. Kamide, T. Ogawa, and Y. Yamamoto, Phys. Rev. B **91**, 115129 (2015).
- [53] G. Stefanucci and R. van Leeuwen, *Nonequilibrium Many-Body Theory of Quantum Systems: A Modern Introduction* (Cambridge University Press, Cambridge, UK, 2013).
- [54] Y. Matsuda and H. Shimahara, J. Phys. Soc. Jpn. **76**, 051005 (2007).
- [55] H. Hu and X.-J. Liu, Phys. Rev. A **73**, 051603(R) (2006).
- [56] J. J. Kinnunen, J. E. Baarsma, J.-P. Martikainen, and P. T3rm3, Rep. Prog. Phys. **81**, 046401 (2018).
- [57] We note that the parameter μ in Eq. (28) is given by the filling of the reservoirs, see Fig. 1.
- [58] D. Bohm, Phys. Rev. **75**, 502 (1949).
- [59] Y. Ohashi, and T. Momoi, J. Phys. Soc. Jpn. **65**, 3254 (1996).
- [60] K. V. Samokhin and B. P. Truong, Phys. Rev. B **96**, 214501 (2017).
- [61] G. Baym and L. P. Kadanoff, Phys. Rev. **124**, 287 (1961).
- [62] Although the last term in Eq. (69) may affect the dynamics of quantities obtained without taking the \mathbf{p} -summation, such as the pair amplitude given by Eq. (81), the following discussion will not handle the dynamics of such quantities.
- [63] J. B. Ketterson and S. N. Song, *Superconductivity* (Cambridge University Press, Cambridge, 1998), Chap. 49.
- [64] A. F. Andreev, Zh. Eksp. Teor. Fiz. **46**, 1823 (1964) [Sov. Phys. JETP **19**, 1228 (1964)].
- [65] The Moyal product in Eq. (56) involves the product of \mathbf{p} -derivative and \mathbf{r} -derivative, such as $\overleftarrow{\partial}_{\mathbf{r}} \cdot \overrightarrow{\partial}_{\mathbf{p}}$. While the \mathbf{r} -derivative is on the order of $|\mathbf{q}|$, the \mathbf{p} -derivative is estimated to be p_{F}^{-1} : Since $\Delta_0 \ll \varepsilon_{\text{F}}$ (quasiclassical condition) is satisfied in the BCS regime, the Green’s function is localized at $|\mathbf{p}| = p_{\text{F}}$ in the momentum space. In this

situation, we can fix the magnitude of the momentum at p_F , that is, $\mathbf{p} = p_F \hat{\mathbf{e}}_r + p_\theta \hat{\mathbf{e}}_\theta + p_\phi \hat{\mathbf{e}}_\phi$. Then, the gradient in the momentum space reads $\partial_{\mathbf{p}} = p_F^{-1} \partial_{p_\theta} \hat{\mathbf{e}}_\theta + (p_F \sin \theta)^{-1} \partial_{p_\phi} \hat{\mathbf{e}}_\phi$, and one can see that the \mathbf{p} -derivative is on the order of p_F^{-1} (see [66] for more general and longer discussion). Thus, the terms arising from $\overleftarrow{\partial}_r \cdot \overrightarrow{\partial}_{\mathbf{p}}$ are of order $|\bar{\mathbf{q}}|/p_F$, and the first-order gradient approximation explained below Eq. (56) will hold well when $|\bar{\mathbf{q}}|/p_F \ll 1$ is satisfied.

[66] N. B. Kopnin, *Theory of nonequilibrium superconductiv-*

ity (Oxford University Press, 2001).

[67] G. Sarma, J. Phys. Chem. Solids **24**, 1029 (1963).

[68] W. V. Liu and F. Wilczek, Phys. Rev. Lett. **90**, 047002 (2003).

[69] I. Snyman and Yu. V. Nazarov, Phys. Rev. B **79**, 014510 (2009).

[70] I. V. Bobkova and A. M. Bobkov, Phys. Rev. B **89**, 224501 (2014).

[71] J. A. Ouassou, T. D. Vethaak, and J. Linder, Phys. Rev. B **98**, 144509 (2018).